Presented at Symposium on
Medical Radioisotope Scintigraphy,
Monte Carlo, October 23-28, 1972

IAEA/SM-164/161
(LBL-1328)

CLINICAL AND RESEARCH QUANTITATIVE NUCLEAR MEDICINE SYSTEM

Thomas F. Budinger

Donner Laboratory and Lawrence Berkeley Laboratory
University of California
Berkeley, California

October 1972

AEC Contract No. W-7405-eng-48

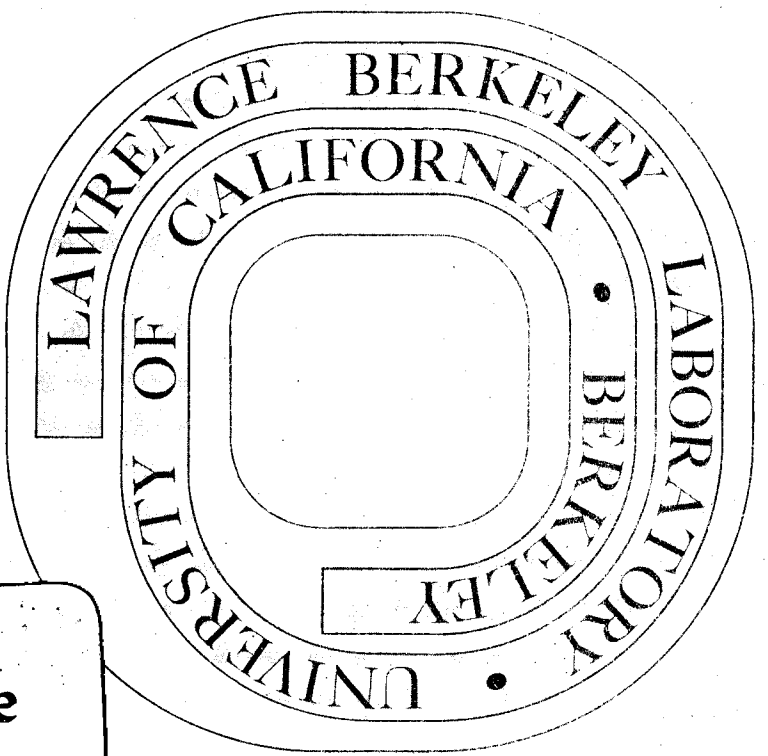

DISCLAIMER

Presented at Symposium on
Medical Radioisotope Scintigraphy,
Monte Carlo, October 23-28, 1972

IAEA/SM-164/161
(LBL-1328)

CLINICAL AND RESEARCH QUANTITATIVE NUCLEAR MEDICINE SYSTEM

Thomas F. Budinger

Donner Laboratory and Lawrence Berkeley Laboratory
University of California
Berkeley, California

October 1972

AEC Contract No. W-7405-eng-48

48

CLINICAL AND RESEARCH QUANTITATIVE NUCLEAR MEDICINE SYSTEM

Thomas F. Budinger
Donner Laboratory and Lawrence Berkeley Laboratory
University of California
Berkeley, California

ABSTRACT

The spatial and temporal resolution of digital computer systems interfaced to gamma cameras and other nuclear medicine imaging devices are not adequate for clinical or research investigations. Data losses as great as 40% occur during dynamic heart studies, and the gamma camera spatial resolution cannot be adequately represented by systems with 32×32 or 64×64 rasters. A system comprising analog to digital conversion in 3 μsec with data accumulation in list mode at 82 kHz, and in histogram mode at 300 kHz, is now available for clinical and research studies. Frame rate is 100 per sec in list mode. This disc operating system uses the Hewlett-Packard 2100A computer (16-bit words) and movable head discs (2.4 million words) with CRT display and light pen for assistance in generating time-activity curves.

For the camera the usual acquisition resolution is 128×128, but can be 256×256. The routine display is 64×64, with the ability to present 128×128 images. The whole-body scan is represented by six frames (64×384) and four isotopes for transmission-emission whole-body isotope quantitation. At one time 160 images and 16 time-activity curves are available for immediate access for display or arithmetic manipulations. Programs implemented on this system with 12K memory include one- and two-dimensional Fourier transforms, washout or clearance images, and rapid means of adding, subtracting, multiplying, and dividing images or time-activity curves by other images or time functions or by scalers. The system can be operated by a technician or clinician with no prior computer experience. The Anger whole-body scanner consisting of a bed which moves over an array of 64 NaI(Tl) detectors has been interfaced to this digital system as well as the Anger scintillation camera operating at 3 μsec pulse pair resolution. Examples of dynamic and static studies of brain, heart, kidneys, pancreas, and bone are shown, using both conventional display techniques and display of functional images where time and isotope relationships are coded by color.

1. INTRODUCTION

Quantitative nuclear medicine or dynamic nuclear medicine using imaging devices such as rectilinear scanners or Anger scintillation cameras has been limited because of inadequacies in the hardware and software for data acquisition, manipulation, and display. The system now in use at Donner Laboratory on scintillation cameras and the Anger whole-body scanner (Figs. 1 and 2) was designed to overcome limitations in temporal and spatial resolution as well as limitations in user experience and computer skills. The system characteristics and design specifications are based on the experience, ideas, and inventiveness of nuclear medicine researchers and clinicians who developed systems of their own or have published their experiences with commercial computers or multichannel analyzer systems [1-21]. The new generation systems I have reviewed* suffer from inadequate display techniques, and most systems lack adequate temporal and spatial resolution for data acquisition and storage. At the time of this writing the Hewlett-Packard system (5407A) has a speed of data handling with spatial resolution of 128×128 and flexibility not yet present in other systems to my knowledge.

The data acquisition and manipulation characteristics were designed to provide a base from which all known or published nuclear medicine procedures could be effected. Mere digitation is not quantitation, and thus a truly quantitative system requires characteristics in excess of those available commercially in small systems. The computing power of small 12K, 16-bit word machines should include the ability to do one- and two-dimensional Fourier transforms [22], tracer kinetics modelling [23, 24], fractional clearance washout images, and three-dimensional reconstruction—as well as routine dynamic flow studies of brain, lungs, heart, and kidneys and special studies such as ejection fraction and cardiac shunts. The basic problems most systems share in dynamic function evaluation are adequate speed without loss of spatial resolution and computational speed with flexibility. Arguments regarding the merits of large vs. small computers disappear when one does on a small computer system timely calculations usually relegated to a large machine, such as two-dimensional integral transforms.

---

*Major commercial systems which use digital data acquisition through computers or analyzers are Baird Atomic, Digital Equipment Corporation, Hewlett-Packard, Intertechnique, Medical Data Systems, Nuclear Chicago, and Nuclear Data.

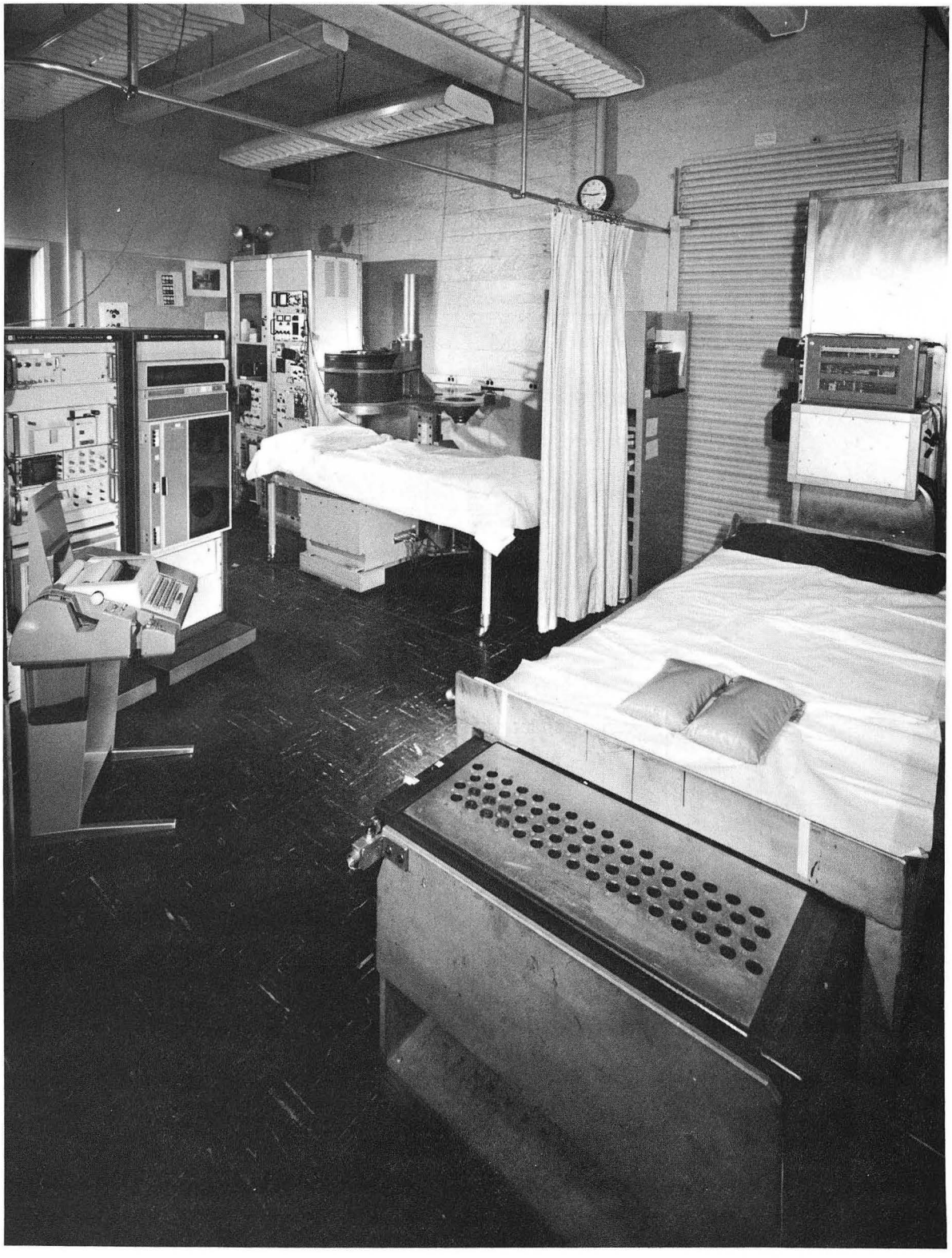

Fig. 1. Part of the nuclear medicine facilities at Donner Laboratory, showing the whole-body scanner (foreground) and small Anger camera interfaced to the HP-5407 digital system.

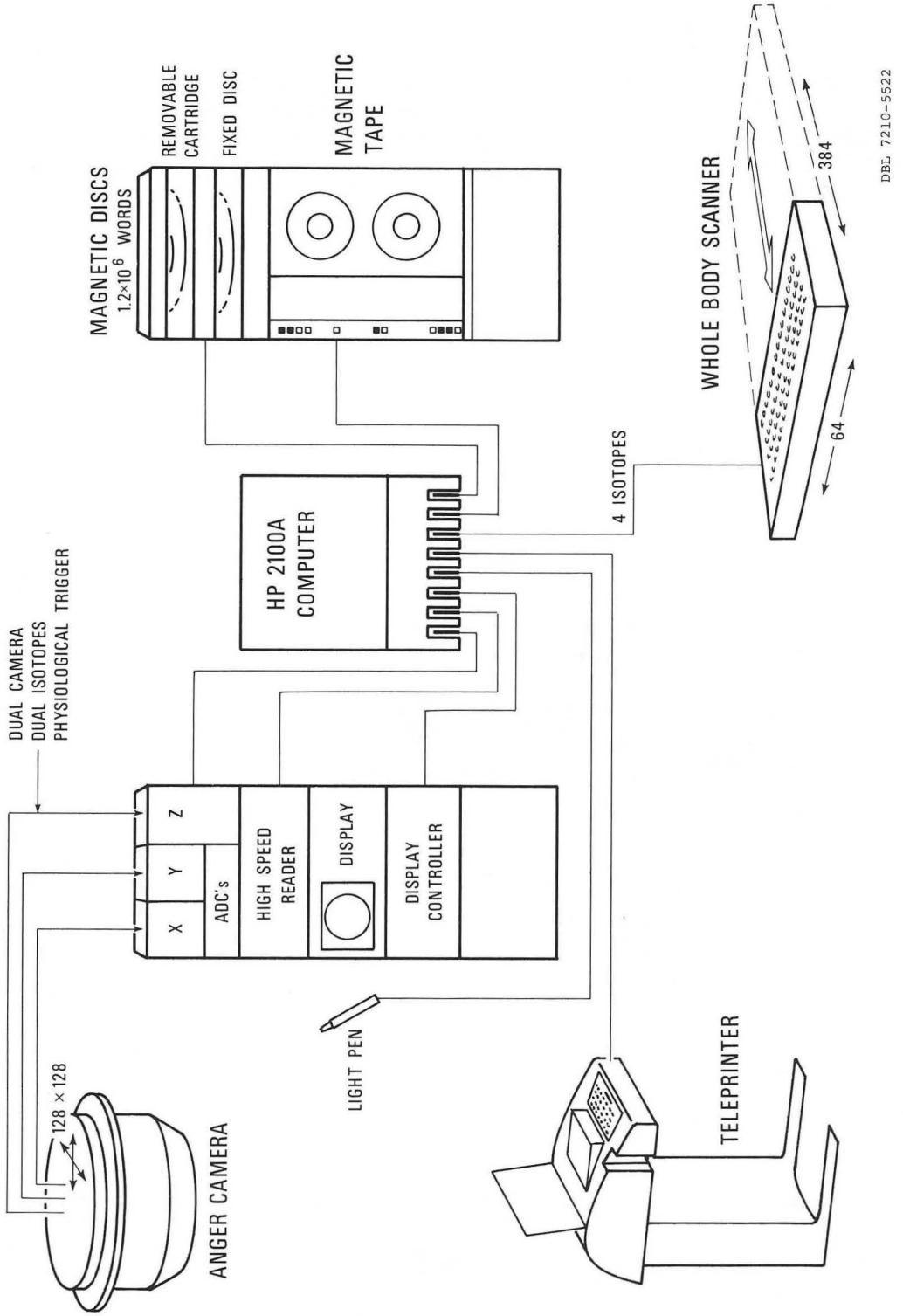

Fig. 2. Schematic of the digital system configuration. All parts of this system except the whole-body scanner interface are now commercially available.

The purpose of this paper is not so much to describe a nuclear medicine computer system, but mainly to clarify the rationale and importance of the essential ingredients which comprise a flexible quantitative nuclear medicine system which can be used by both clincian and researcher as a tool for medicine. Because relevant literature is cited wherever possible, some of this work also serves as a guide to the clinical and research literature.

2. HARDWARE AND SOFTWARE DATA CONTROL

2.1 Analog to digital conversion

The conversion from analog position signals to digital words is one of the most crucial parts of the system because here the camera data can be distorted and lost without the clinician or researcher knowing that his poor computer results are not the result of a poor study with bad statistics, but the result of spatial and temporal data distortion. There are five characteristics desirable for a nuclear medicine ADC:

Pulse pair resolution <3 μsec,
Differential nonlinearity $<1\%$,
7-bit digitization in X and Y (128×128),
Ability to move field of view
Ability to zoom.

Speed and spatial resolution requirements are vital to any quantitative nuclear medicine system. The argument that 3 μsec is faster than the camera is not valid, because commercial imaging systems can be made to operate with 3 μsec dead time and really should be improved to this speed because of the serious data loss during dynamic studies (Fig. 3). During the routine 10 mCi ^{99m}Tc-pertechnetate or albumin cardiac study, the data rate of photopeak events is 40 kHz during 2 to 3 seconds of the study. With a dead time of 20 μsec the loss of data is 30%; for 40 μsec, 50%. A processing system whose pulse pair resolution is longer than the input data time resolution effects data losses which depend on the dead time τ, input data rate R_t, and probability density function of the data source. For a Poisson source, this data loss is [25]

$$\text{Fractional loss} = \frac{1-e^{-R_t\tau}}{R_t \cdot \tau} . \tag{1}$$

This expression is derived from the fact that the probability one or more events occur in a time window of τ for a count rate of R_t is just

$$1 - e^{-R_t\tau} . \tag{2}$$

The observed count rate is

$$R_0 = \frac{1 - e^{-R_t\tau}}{\tau} \tag{3}$$

which differs from the conventional expression [26]

$$R_0 = \frac{R_t}{R_t\tau + 1} . \tag{4}$$

The latter expression is a valid approximation for non-Poisson distributed

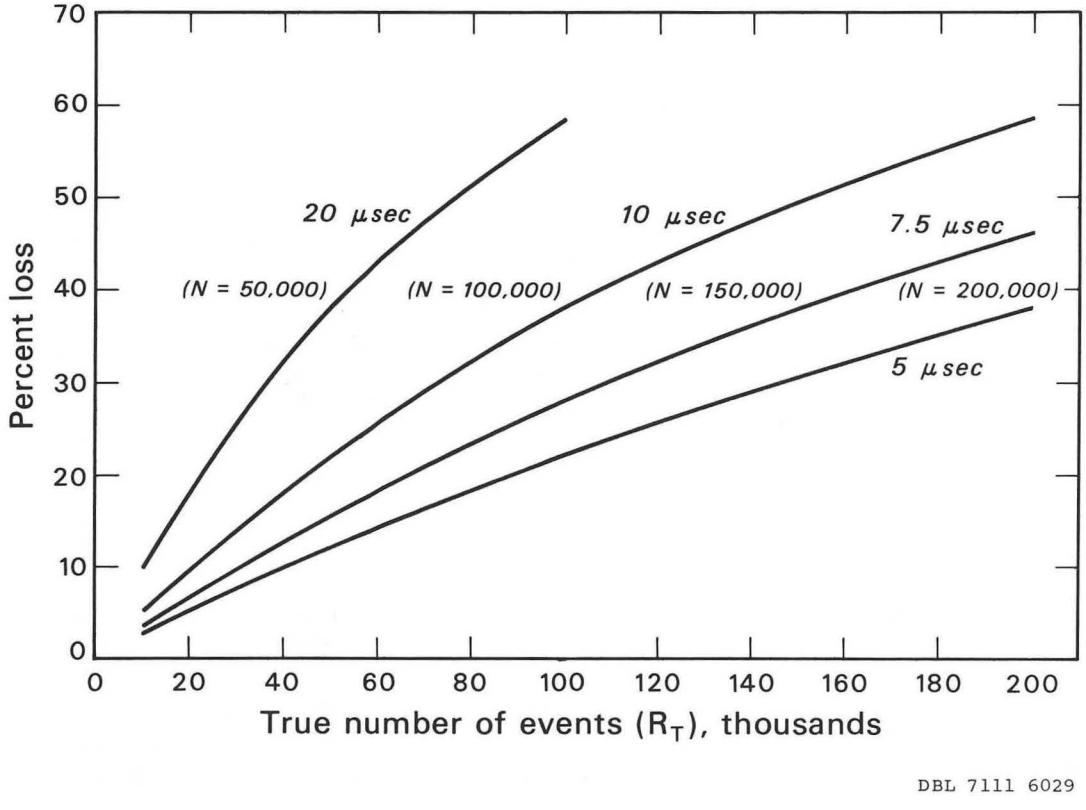

Fig. 3. Percent data loss for various dead times. Most systems have an effective dead time of 20 μsec.

input, which is probably the case for count rates over 30 000 from the scintillation camera. The clock time of the dual ADC's used in the Hewlett-Packard 5407 system is 200 MHz, and the pulse pair resolution for each ADC digitizing 7-bits is 3 μsec. Slower systems not only limit statistics, but give washout or flow curves which are distorted and must be corrected before they can be used for quantitative work. Correction of the observed counts to the true counts in some interval of time is dangerous because the basic statistics cannot be improved.

The law of propagation of errors [27] can be used to show that the variance of the calculated count rate is related to the variances in observed count rate and the variance in the dead time measurement,

$$\text{var}(R_t) = \left(\frac{\partial R_t}{\partial R_0}\right)^2 \text{var}(R_0) + \left(\frac{\partial R_t}{\partial \tau}\right)^2 \text{var}(\tau) \tag{5}$$

if there is no dependence of the dead time on the count rate. From Eq. (5) and Eq. (4) one can show the standard deviation of a corrected count, N_c, for a time interval, T, on a system with dead time, τ, will be

$$\sigma(N_c) = \sqrt{N_c}\left[1 + \frac{2N_c^3 \text{var}(\tau)}{T^2}\right]^{1/2} \tag{6}$$

Thus the error is greater than merely $\sqrt{N_c}/N_c$ but, as shown by Heiss and co-workers [20], this error is less than the error which might be expected from the observed statistic $\sqrt{N_0}/N_0$.

A calculation of the effect of data dropout is shown in Fig. 4, where an uptake-washout curve is simulated for 0, 20, and 40 μsec dead times. A few levels of analog derandomization buffers [19] will effectively increase the analog to digital conversion speed capacity. Multicrystal NaI(Tl), multiwire gas or liquid-filled Xe proportional chambers, or pure germanium cameras can easily provide data at rates of 1 MHz. We should look to the ADC with 2 μsec pulse pair resolution, then add analog and digital buffers, as needed. Eventually we will need solid state memory devices when isotopes of short half-life become used in 40 mCi amounts. The limiting factor in the near future will be computer cycle time; however, at present ADC pulse pair resolution seems to be the nuclear medicine bottleneck for fast dynamic studies.

The spatial or energy resolution of an ADC is designated by the bits digitized; e.g., 64 is 6 bits and 128 is 7 bits. The argument for setting up a system with a resolution of 64×64 or 32×32 is that it is convenient for a particular 12-bit and 16-bit word computer. As has been shown by Erickson and Brill [28] from the changes in the modulation transfer function, one needs more than 64×64 elements across a 25.4 cm crystal. Consider another argument for array size. If a 25.4 cm crystal can resolve a sinusoidal wave of 0.8 cm wave length, we expect 25.4/0.8 = 31.7 wave lengths or cycles. The uniform sampling theorem in the spatial domain asserts that if a real space function, f(x), contains no frequency components greater than S_{max} cycles per unit distance, then f(x) can be completely determined by its values at uniform intervals less than $(2 \times S_{max})^{-1}$. Thus for 0.8 cm resolution we need 63 sample points, and for 0.5 cm resolution we need 102 sample points. The resolution

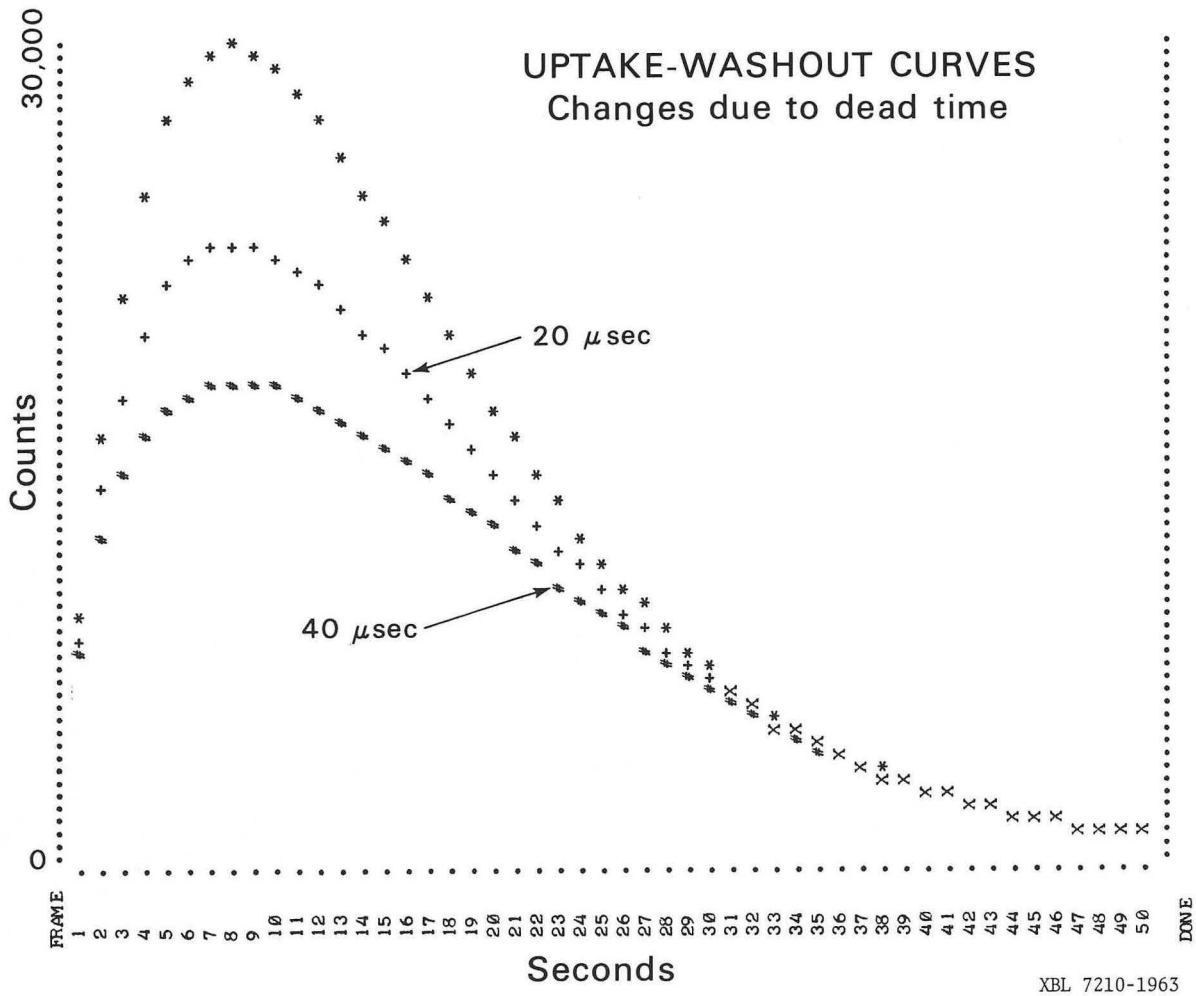

Fig. 4. Uptake-washout curves for study where the ADC pulse pair resolution is negligible compared to realistic situations where the processing times are 20 and 40 μsec. Peak count rate was 29 000.

pattern is not a simple sine wave, and higher order components comprise the bar pattern frequency spectrum. A resolution greater than 100×100 is required for faithful reproduction of camera images as shown in Fig. 5; thus a system limited to 64×64 resolution is unlikely to gain general acceptance in the next few years. Array sizes of 128×128 necessitate four times more storage and four times more speed than needed for conventional 64×64 arrays. Techniques other than histogram accumulation of 16K arrays in the central processor can provide 128×128 arrays without large investments in memory devices. These techniques include the use of list mode accumulation, and the ability to zoom the ADC. Use of list mode accumulation allows one to acquire data with spatial resolution limited only by the computer word size and resolution of the ADC (8-bit ADC = 256 point resolution). The basic configuration we use allows us to digitize 128×128. With a wire jumper change in the ADC format board we can digitize 256×256 but would have to change our time mark convention. Another technique of realizing the inherent resolution of a camera is the technique of zooming the ADC's to examine a small portion of the crystal with high spatial resolution. This capability is available on many ADC's but the analog gain and offset controls are usually not readily accessible. Use of a pinhole collimator does not accomplish the same purpose because the inherent crystal resolution is still not fully ulitized if a 25 cm diameter area is represented by only 64×64. By zooming we digitize a smaller area with 64×64 or 128×128, as shown in Fig. 5 for a bar pattern whose 6.35 mm (1/4 inch) resolution quadrant is shown at a spatial digital sampling resolution of 64×64, 128×128 and, through zooming, 300×300.

2.2 List mode vs. frame or histogram mode

The list mode accumulation means each count is stored by signifying the X and the Y position information sequentially (in a list) as the counts arrive from the camera. Thus an 80 000-dot picture would be represented by 80 000 computer words--the difference between each word being the position coordinates of each event. The frame or histogram mode implies that each count is placed in its appropriate position in a two-dimensional array of, for example, 64×64 or 128×128. The computer location representing a particular position in the frame (on the crystal) is incremented by one count each time an event arrives from that position. Thus the frame or histogram mode gives an integrated picture of the isotope distribution. The integration period depends on the frame rate, which is usually greater than 10 sec^{-1}. This mode of operation is equivalent to 35 mm, Polaroid film, or storage scope picture accumulation which is available on commercial camera systems. For the full benefit of gamma camera nuclear medicine studies using small computers, list mode is necessary because it allows high spatial resolution imaging with high temporal resolution. List mode allows higher frame rates than obtainable with histogram mode. Framing speed is achieved in our system by inserting time markers every 10 msec during data accumulation. Thus in list mode, frames of 128×128 can be obtained at frame rates of 100 sec^{-1}. Appropriate electronic modifications can improve camera rates to 100 kHz, and meaningful physiologic data can be obtained with frame rates of 20 sec^{-1} with 128×128 resolution. Because each count has to pass through the entire system (ADC → computer core → storage), list mode data rates are limited by the acquisition speed of the slowest component. Disc or drum data accumulation systems have the required speed; tape systems are too slow for list mode operations. The limit for 45 ips 9-track tape is about 30 kHz and the limit for a movable head disc system (less than $20 000) is about 80 kHz.

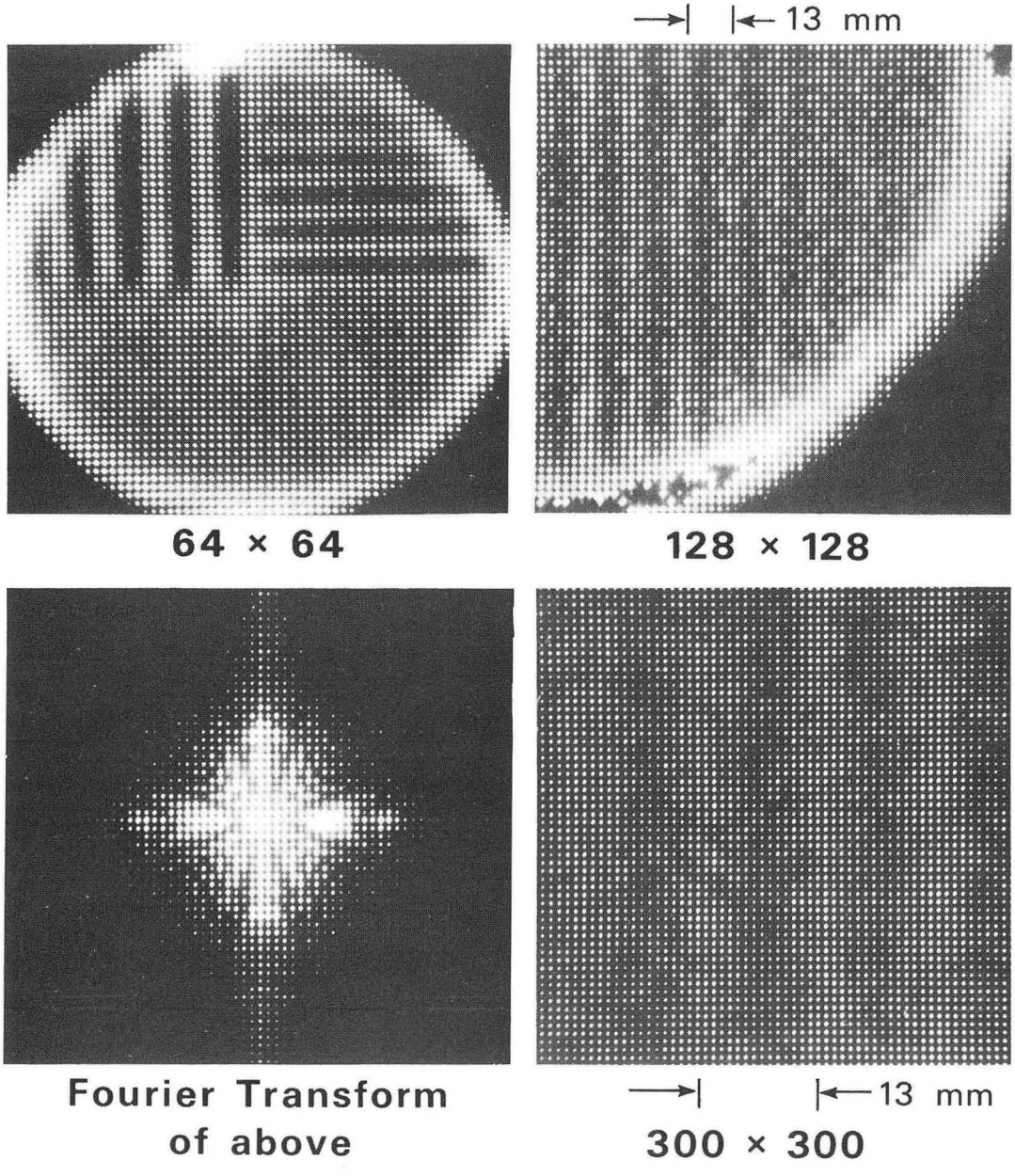

Fig. 5. Illustration of the inadequacy of 64×64 resolution digitalization. Right lower quadrant of 6.35 mm wide bar pattern was digitized at 128×128 in right upper figure, and the same pattern was digitized with a resolution of 300×300 by using the zoom control of the ADC's. Fourier transform shows the power spectrum of the entire bar pattern.

On the other hand, fast data rates in the order of 300 kHz can be accommodated by histogram mode because the bulk frame data accumulated from t_1 to t_2 can be transferred to storage while a successive frame is being accumulated during t_2 to t_3 in another 4K section of computer memory. Further, histogram storage of a 64×64 frame requires only 4096 words. Thus in the case of a 100 000-event study the capacity for total counts is greater by a factor of 25 in histogram mode. However, there are two reasons why a fast, say 20-frame per second, histogram mode will not suffice for nuclear medicine studies. First, we do not get sufficient spatial resolution with the small memories of 12K or 16K which are economically available in small machines or data transfer systems. To transfer frames of 128×128 elements in histogram mode at high data rates requires a core of 2×(128×128) + 4K = 36K. Some yet untested techniques of core splitting have potential for reducing this large core requirement. Secondly, fast dynamic studies in histogram mode are likely to fail unless the duration of accumulation is timed relative to the timing of isotope movement in the area of camera view. An example will clarify this statement. Suppose a 10 mCi ^{99m}Tc cardiac dynamic study is to be made at a 64×64 frame rate of 20 sec^{-1}, and the computer accumulation commences at the time the isotope is injected. Assume that after 6 seconds the isotope center of gravity is in the right heart. We have used up 4096 ×6×20 words or more than one-third of a 1.2-million 16-bit word disc. After another 8 seconds we find the bolus in the left ventricle, and our rapid storage device is nearly full. If it is 10 seconds before the isotope is in the right heart (a common occurrence), then we would run out of storage before the left ventricle is visualized. High speed tapes can be used as mass storage; however, they are inappropriate because the usual tape transports will not allow data transfer faster than about 30 kHz, and at the most interesting part of a cardiac study as much as 25% of the useful data will be lost in addition to that lost from system dead time discussed above.

List mode accumulation is used on analog systems using magnetic tape with analog playback. These systems have only limited data manipulation capabilities, and less than one-half the speed of digital, list mode disc systems. Further, they do not have the precise time mark capability of digital systems. They do have the capability to do irregular area of interest dynamic functions by using photodiode [29] or photomultiplier tubes [30] which view a masked-off area of the video screen during playbacks.

The attributes of several modes of data accumulation are tabulated below. An asterisk signifies a particular mode is superior to others in the same category without an asterisk. Obviously the ideal system will have both histogram and list mode. Once the data have been accumulated in list mode, they must be framed for viewing (Fig. 6). Raw data accumulation is made on a 1.2-million word raw data disc, from which data can be framed in time increments of 10 msec and greater. Our system requires 400 msec to frame from a list of events stored on disc to a 4K frame. The frame file is for 4K words, usually as 64×64 frames, but these frames can also be 32×128, since the X and Y data are stored as 7×7 bits and can be reframed by a simple typed message for change in format. Thus one can reframe raw data into 4 frames, each 32×128, giving an aggregate 128×128 or 4 frames of 64×64 representing 4 quadrants of a 128×128 frame.

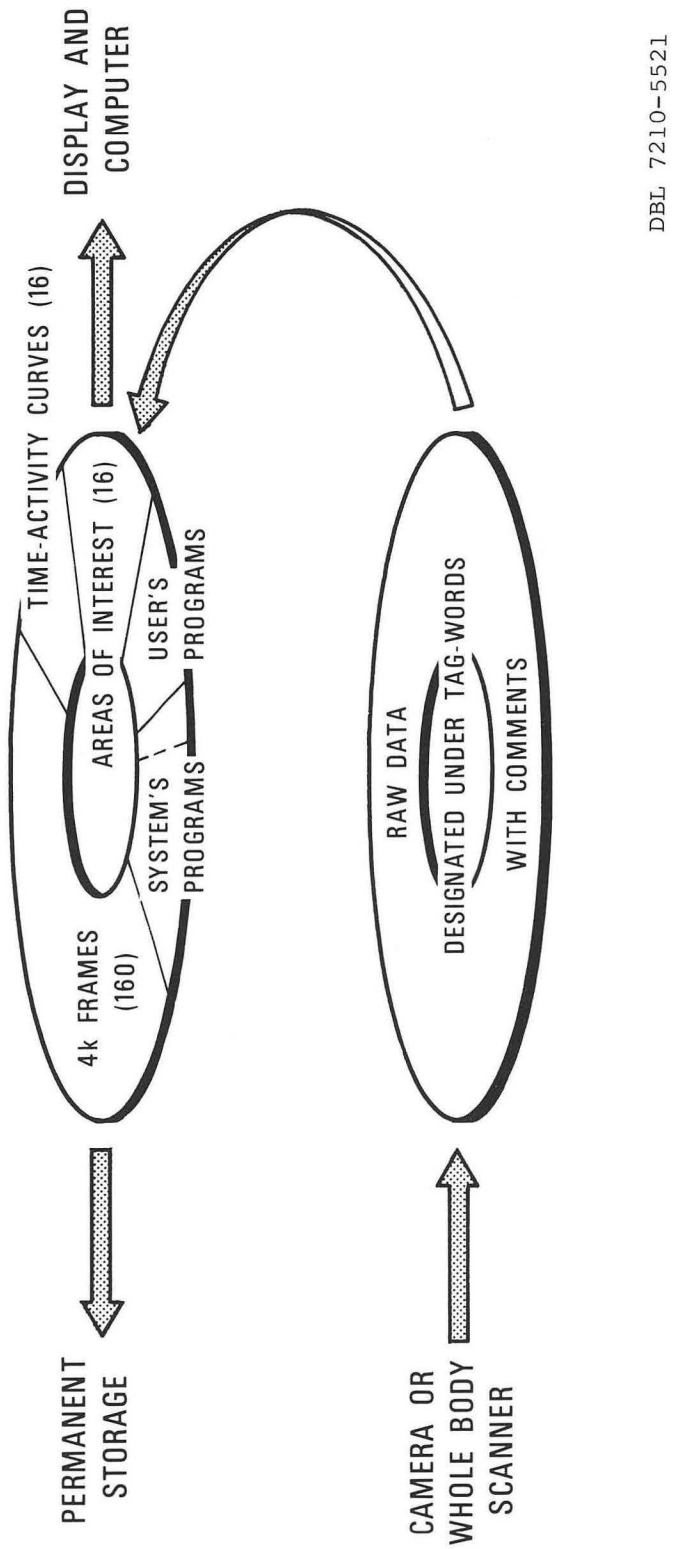

Fig. 6. The data flow from ADC or whole-body scanner to raw data disc in list mode or histogram mode. Data are framed into any one or a series of 160 available frames in the removable cartridge disc, which also contains system's and user's programs.

	Count rate	Frame rate	Resolution	Dynamic storage economy	Static storage economy
List mode		*	*	*	
Histogram mode	*				*
Analog list mode			*	*	

The time intervals between frames is based on the user needs. List framing for slow or medium speed (200 msec) studies is preferred over histogram framing, because the interval chosen for framing cannot be less than the histogram interval selected before the commencement of the study and, as emphasized above, we have 4 times the spatial resolution in list mode.

2.3 Rationale and specifications for a disc

Systems without a fast storage device, such as a disc or drum, leave the nuclear medicine clinician with a severe handicap, not only in the work of dynamic imaging, but in the speed and convenience of moving programs and frames from one place to another. The disc gives a small computer the capabilities of larger machines. A disc is a memory device similar in size to a phonograph record, but made of aluminum and coated with iron oxide particles suspended in an organic binder. In movable head discs there is a transducer which moves in and out over the rotating platter. This head magnetizes the disc portion over which it is programmed to be in accordance with the presence or absence of information being transferred from core. Data are read by sensing the magnetic field on the disc, analogous to a phonograph pickup sensing a ridge in the record groove (track). Fixed head discs have a head per track, and can transfer data much faster than movable head discs, but they cost almost as much as extending computer core (about 10 times the cost of movable head discs). Movable head discs have adequate speed and capacity for nuclear medicine applications to over 50 000 events/sec in list mode, and 300 000 events/sec in histogram mode. The Hewlett-Packard Model 7900A unit consists of two movable-head 1.2-million word (16-bit) discs, one fixed and one an interchangeable cartridge.

The system now has both a fixed and a removable disc cartridge with a total capacity of 40 million data-bits. The fixed disc is used for temporary storage of list mode or histogram mode data, and the removable cartridge is a 1.2-million, 16-bit-word disc which is used as the system's disc with separate "core loads" consisting of acquisition, manipulation, and display system software which are loaded into core as needed. The time to change from one mode of, say, 128×64 display to the time vs. activity curve generation core load is ~ 1 sec. On this removable disc cartridge are 160 frames (4K words) which are fixed spaces on the disc wherein list or histogram raw data can be placed after framing (Figs. 2 and 6). A different removable cartridge disc containing another set of core loads or special routines such as a tomographic scanner system or a whole-body scanner quantitative system can replace the resident disc in less than 60 sec. Thus the individual modes of operation can be changed in the computer by reloading core in 1 sec and the entire system reconfigured to another imaging device, or even a nuclear medicine laboratory management system disc, in less than 60 sec.

2.3.1 Disc speed

The disc rotates at 2400 rev/min. The average single-track seek time is 7 msec, and the average delay is 12.5 msec. The data transfer is 312 000 8-bit bites or 2.5 million bites per second. There are 200 tracks (plus 3 spare tracks) and each track has twenty -four 256-bite sectors.

The system can transfer data at 82 000 words per second. This is done as follows.

Transfer data to track 0 in sectors 0 to 15 (16.7 msec), then move heads to track 1 (17 msec), wait 1.3 msec, then sectors 0 through 15 on track 1 are transferred, and the heads are moved to track 2, and so on for 200 tracks. Now without losing the 55 msec to move the heads 200 tracks back to track 0, the process is repeated starting at track 199. The next data are transferred to sections 16 through 23. The system switches heads and transfers 0 through 15, then 16 through 23 on the other disc surface. This technique allows one to transfer blocks of data at a rapid rate by using a movable-head disc.

2.4 System control

2.4.1 Teletype keyboard control

The mode and language whereby the technician, clinician, or researcher communicates with a system is as important as any other aspect of the system design. The philosophy is to bring the full system including powerful computing capabilities, to the fingertips of a nuclear medicine technician without prior computer or analyzer knowledge or training. Cumbersome computer language or mnemonics have been avoided, and most operations are under the control of a standard ASR-33 teleprinter keyboard which has been labelled by the platten overlay shown in Fig. 7. Explanation of some of the functions is as follows:

CONTROL: (a) Sets the system in idle mode ready to accept a "core load" which consists of a set of instructions for particular modes of operation such as accumulate or display.
(b) Executes a valid command from elsewhere on the keyboard.

ACCUMULATE: A specific core load is read off the disc into computer core thus putting the system in readiness for list mode or histogram mode accumulation of data.

FRAME CREATE: A "core load" which allows the user to transfer raw data into frames of any duration $\geq$ 10 msec, a specified count limitation if desired, and data into frames related to certain physiological markers.

TIME FUNCTION CREATE: When the create key is pressed, a new "core load" enters the system and the user is able to create 1 - 16 time functions consisting of counts integrated over preselected areas of interest. These areas can be overlapping and become part of the permanent record along with the time functions.

FRAME AND TIME FUNCTION ARITHMETIC: User can perform arithmetic operations such as addition,

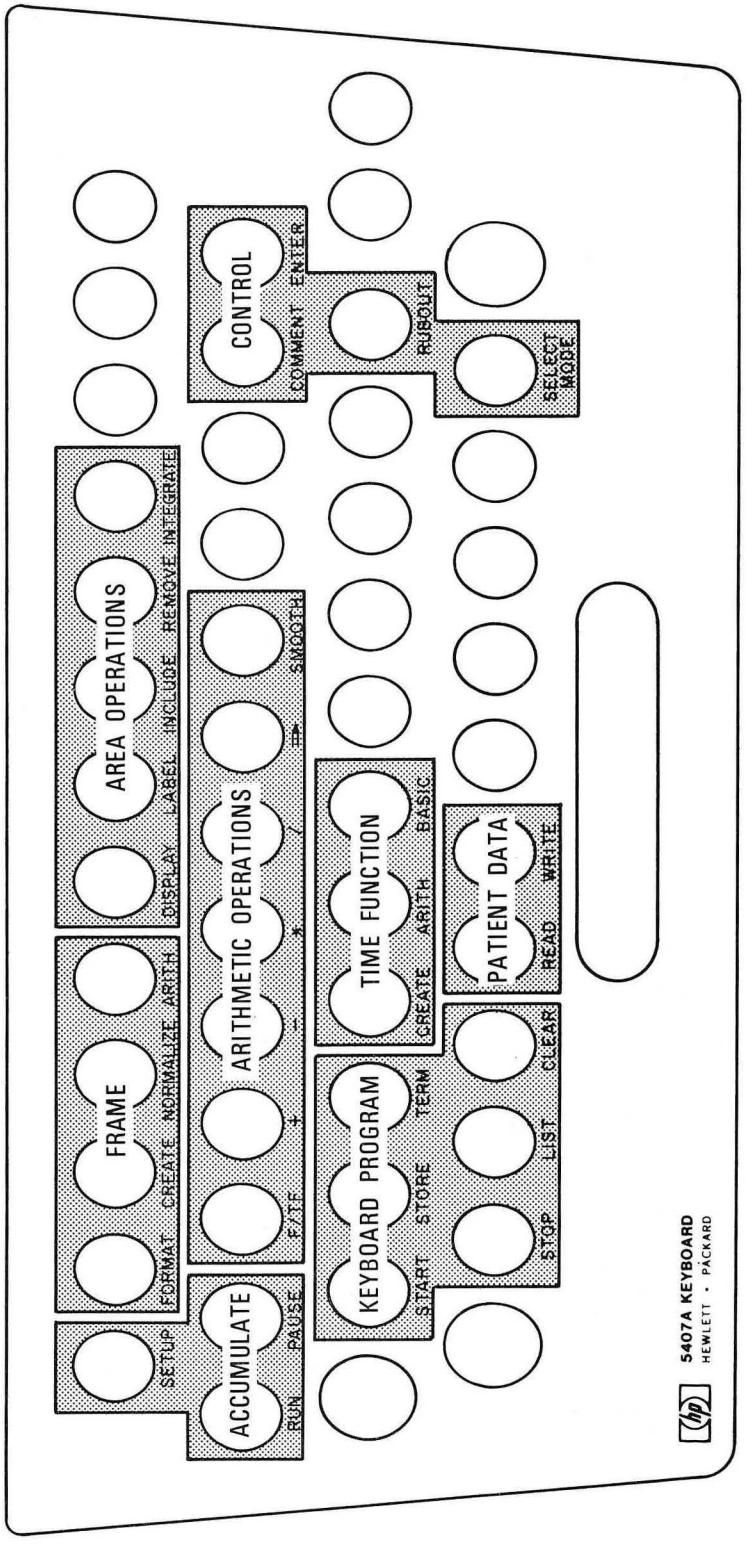

Fig. 7. Teletype keyboard overlap used to denote functions to keys.

subtraction, multiplication and division of one time function or frame by another or by a scaler. These operations take less than 0.5 sec and are performed by simple messages such as

* F1 * 10 → F2

* F2/F3

which means multiply frame 1 by 10 and put the results in frame 2. Then divide frame 2 by frame 3.

BASIC: This key calls in a programming system whereby one can operate on time functions or with user originated programs written in BASIC language.

Some other functions shown in Fig. 7 will be discussed below.

In addition, FORTRAN and ALGOL programs can be written for special manipulations of the frame data which have not already been provided with the system. The fractional clearance (washout) functional image and the Fourier transform programs are FORTRAN special programs added to the basic system.

Thus the teleprinter keyboard serves what appears to be dual functions of command mode messages to the system's programs and the conventional operation of typed messages or parameters to the computer. In the former mode the ASCII-coded input from the teleprinter is picked up from the I/O bus by the computer executive program (keyboard monitor) and an interpreter transforms the ASCII to an internal system language.

2.5 Display

Presentation of the acquired or processed data via computer printout and monochromatic or colored CRT display is usually inadequate because it is not economically feasible to display 128×128 flicker-free on scopes with adequate gray levels by using small computers because each point takes 3 - 4 μsec to display. Storage scopes do not have the gray level capacity or uniform persistence required for nuclear medicine procedures. Storage scopes of 1024×2048 resolution can be used effectively for display of 64×64 by mapping each element from the 64×64 array to an 8×8 or 16×16 subset of the larger array, as has been done successfully in microscopy [25]. Mapping by using a fixed code rather than a random number generator gives a weave pattern which is acceptable, but can be avoided. High-resolution displays can be generated by sweeping out the data on a CRT and integrating the image on film, as is done in scanning microscopy and presentation of moon and Mars pictures after data processing.

We use a HP-180 scope with a P-31 (31 μsec) green phosphor. Our display rate is 40 sec^{-1} for 64×64. This rate usually gives some flicker unless the display algorithm interleaves the rows; this is now done, with excellent results. We have a special program for display of 64×128 which reads out 2 frames (successively) into the display module, and can easily acquire and display 128×128 images by a program which will read 4 frames of 32×128 onto the display screen while the camera shutter is open.

Capabilities of the display are seen in the heart image after injection of ^{129}Cs[31] (Fig. 8). The ability to select count threshold and window as well as the capability of displaying isometric projections are found in most systems. Profiles through any width of X and Y slices allow one to examine the significance of apparent defects, as shown in the study of a defect in a ^{43}K myocardial study from a patient with previous myocardial infarctions (Fig. 9).

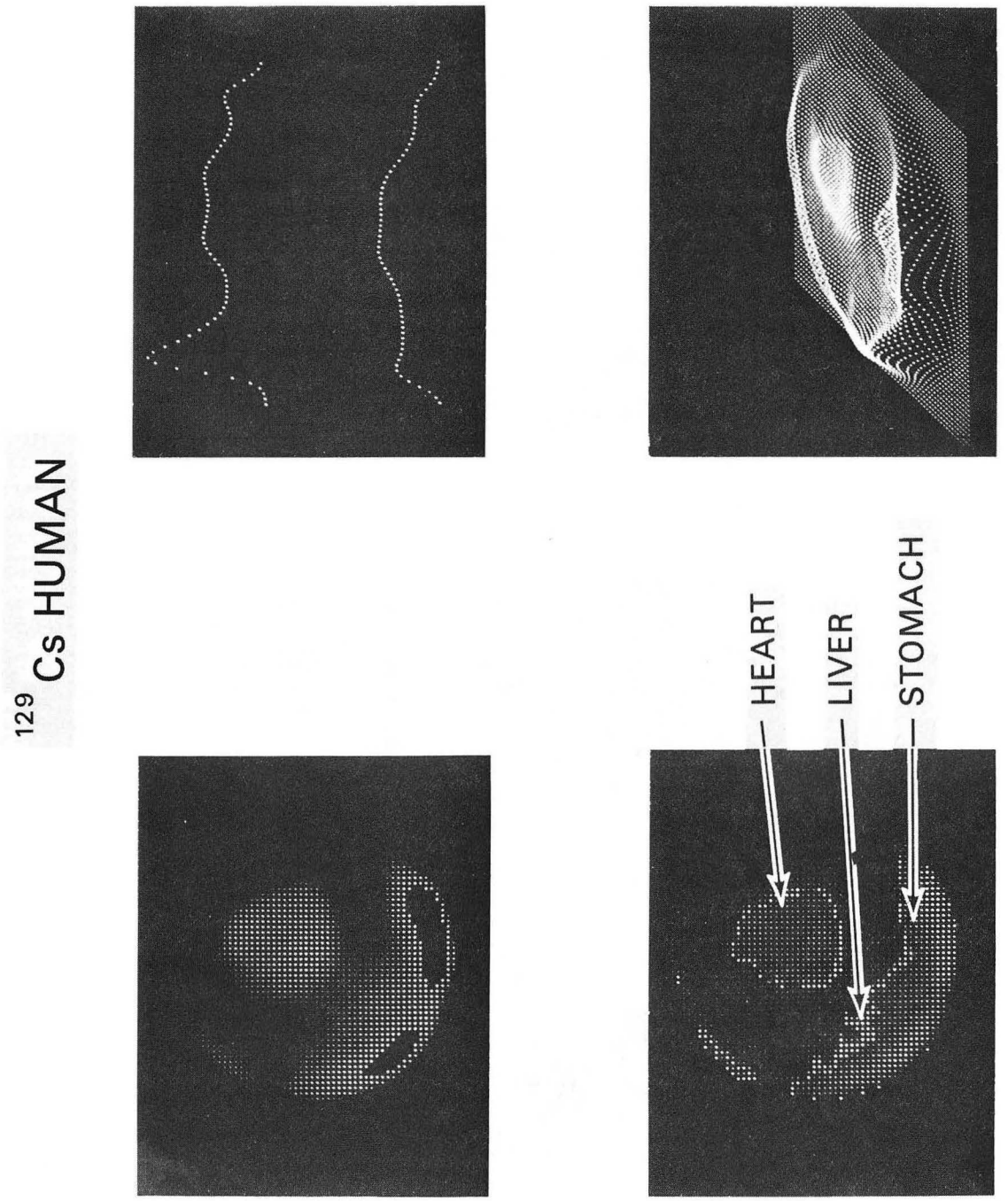

Fig. 8. Heart muscle accumulation of ^{129}Cs after intravenous injection of 500 μCi [31].

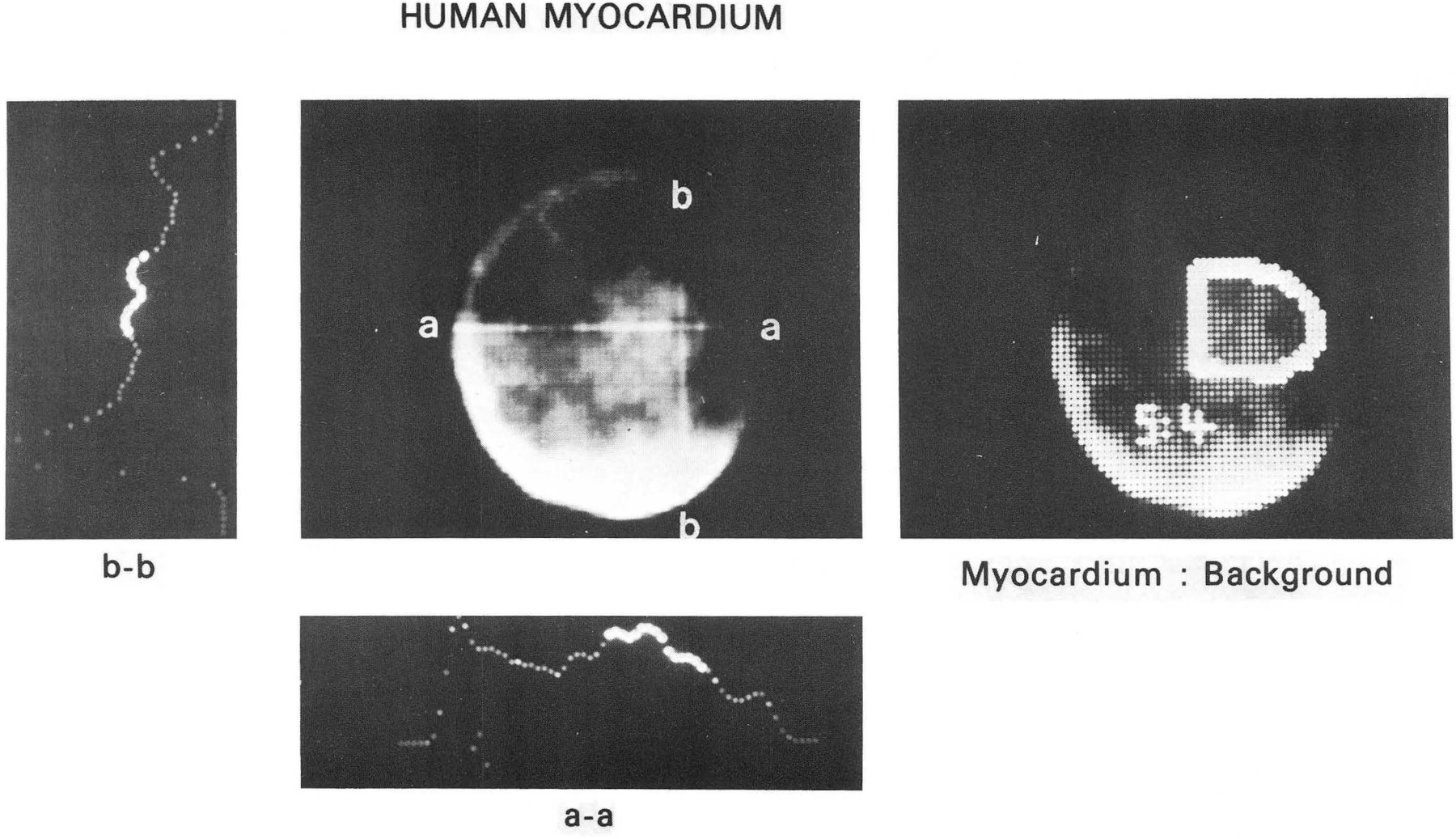

Fig. 9. Profiles through apparent muscle ^{43}K accumulation defect. Image taken 15 min after 500 μCi ^{43}K i. v.

3. IMAGE AND TIME FUNCTION MANIPULATIONS

3.1 Camera and whole-body scanner field nonuniformity corrections

One of the early uses of digital systems on the Anger scintillation camera was to demonstrate the degree of nonuniformity present in many scintillation cameras (frequently variations of 20%). The seriousness of poor camera performance is illustrated by Fig. 10 where an abnormal static ^{99m}Tc-pertechnetate image becomes normal after proper corrections. Quantitative dynamic studies which involve comparison of the flow between parts of the brain, lungs, and kidneys are subject to large errors if proper precautions are not taken to correct the raw data for nonuniformity of camera sensitivity. Symmetry of flow is a useful measure for unilateral brain or vessel pathology; however, here the danger of misdiagnosis is greatest because regional deviations in crystal sensitivity can markedly distort the symmetry of uptake-washout curves of the brain blood flow study. An illustration of this is the abnormal brain flow study which becomes normal when sensitivity corrections are applied (Fig. 11). The camera spatial changes in sensitivity will vary with window width, energy, and symmetry of placement of the window around the photopeak [32, 33]. Figure 12 shows how the nonuniformity varies markedly with placement of the window around the photopeak.

Some techniques of correcting this nonuniformity have been proposed for digital systems [34, 35]. Geometric distortion [36] is far less important than the sensitivity corrections. Nonuniformity corrections must be done in floating point arithmetic. The corrections are done by collecting more than 3 000 000 counts from a uniform source which is larger than the collimated crystal. The correction matrix is applicable to the particular collimator, energy, and window used for the flooded field and subsequent patient study. In order to obtain a normalization matrix with less than 2% standard deviation, it is necessary to accumulate 3 000 000 counts in the inscribed camera circle of a 64×64 array. Because we can expect a 20% deviation from the average, the statistical error in the normalization matrix might be 5%.

The corrected image is obtained as follows:

$$A'_{ij} = \frac{A_{ij} \times \frac{1}{N} \sum_i \sum_j N_{ij}}{N_{ij}},$$

where the numerator is the product of the image counts and the mean value of the flood matrix, and N_{ij} denote the counts in the flood field elements. Zeroes in the flood field are replaced by ones, and zeroes of the image field remain zero. Thus, since a zero count will never be improved upon, one must add one count to all elements before correcting an image with very poor statistics. A better procedure is to tune the camera.

3.2 Fundamental problems in image restoration

The problems of image restoration in nuclear medicine are far more complicated than the problem of planet picture processing NASA has successfully solved. The reason is twofold. First, whereas it is well known that the count rate does not change with distance from the collimator, the

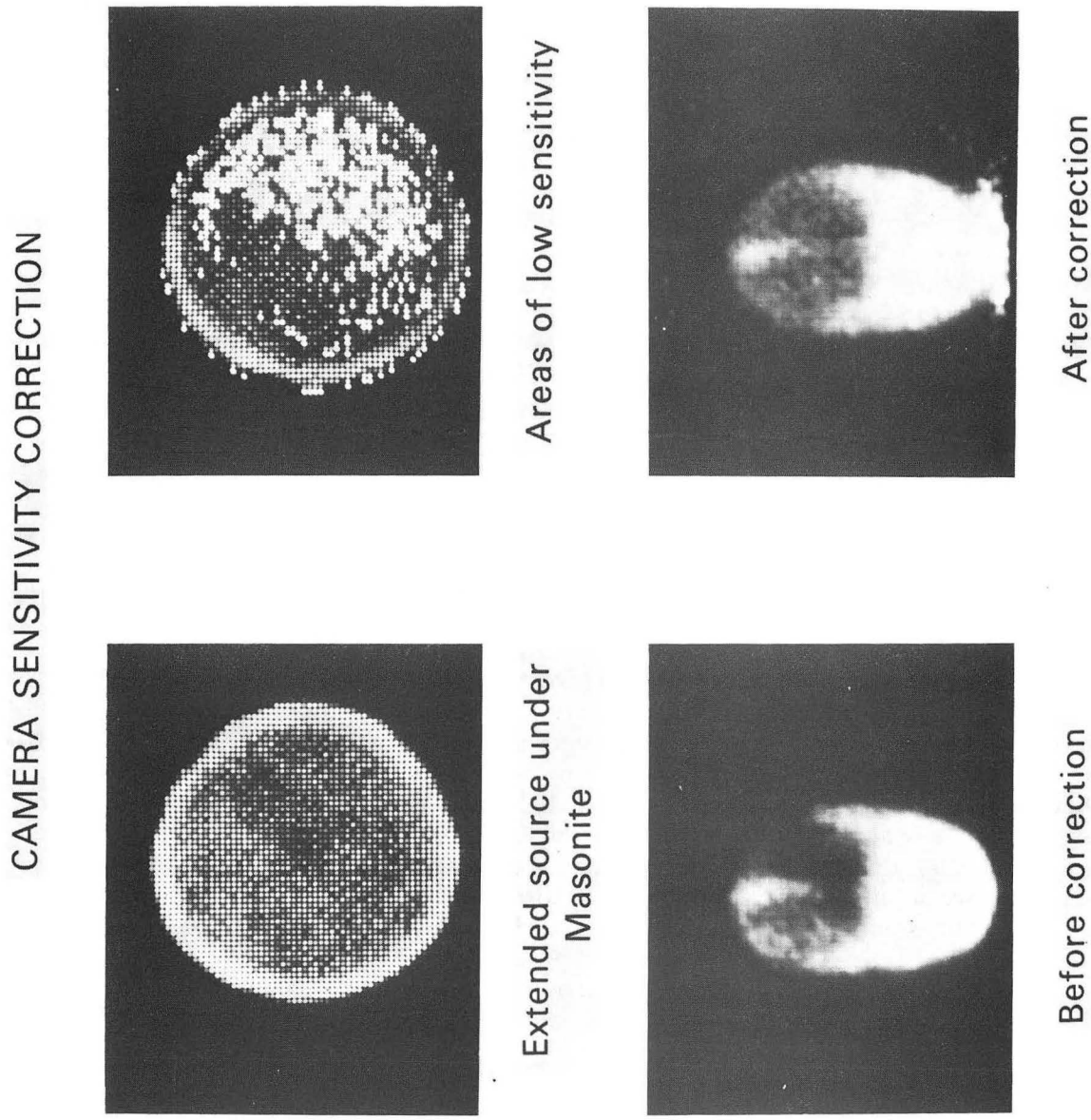

Fig. 10. False positive brain scan due to nonuniform camera response.

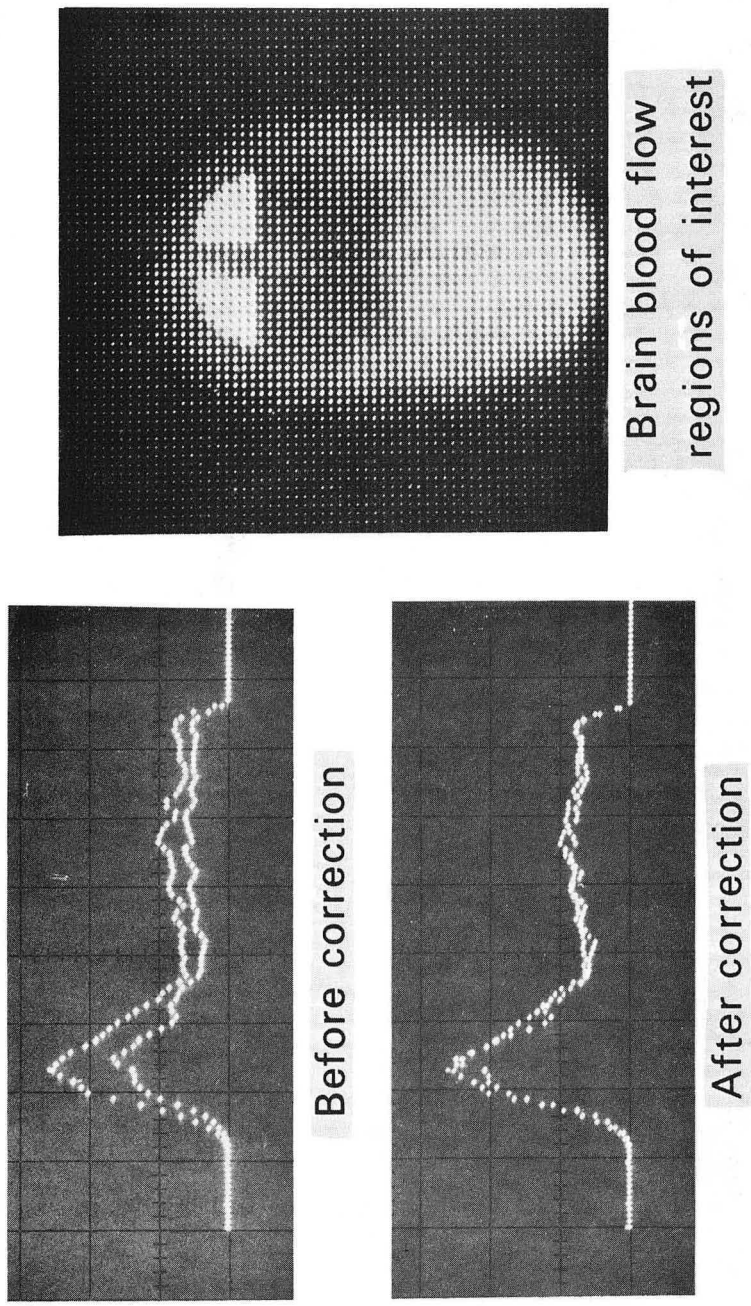

Fig. 11. False positive brain blood flow study corrected by normalization routine based on camera response to a flooded field.

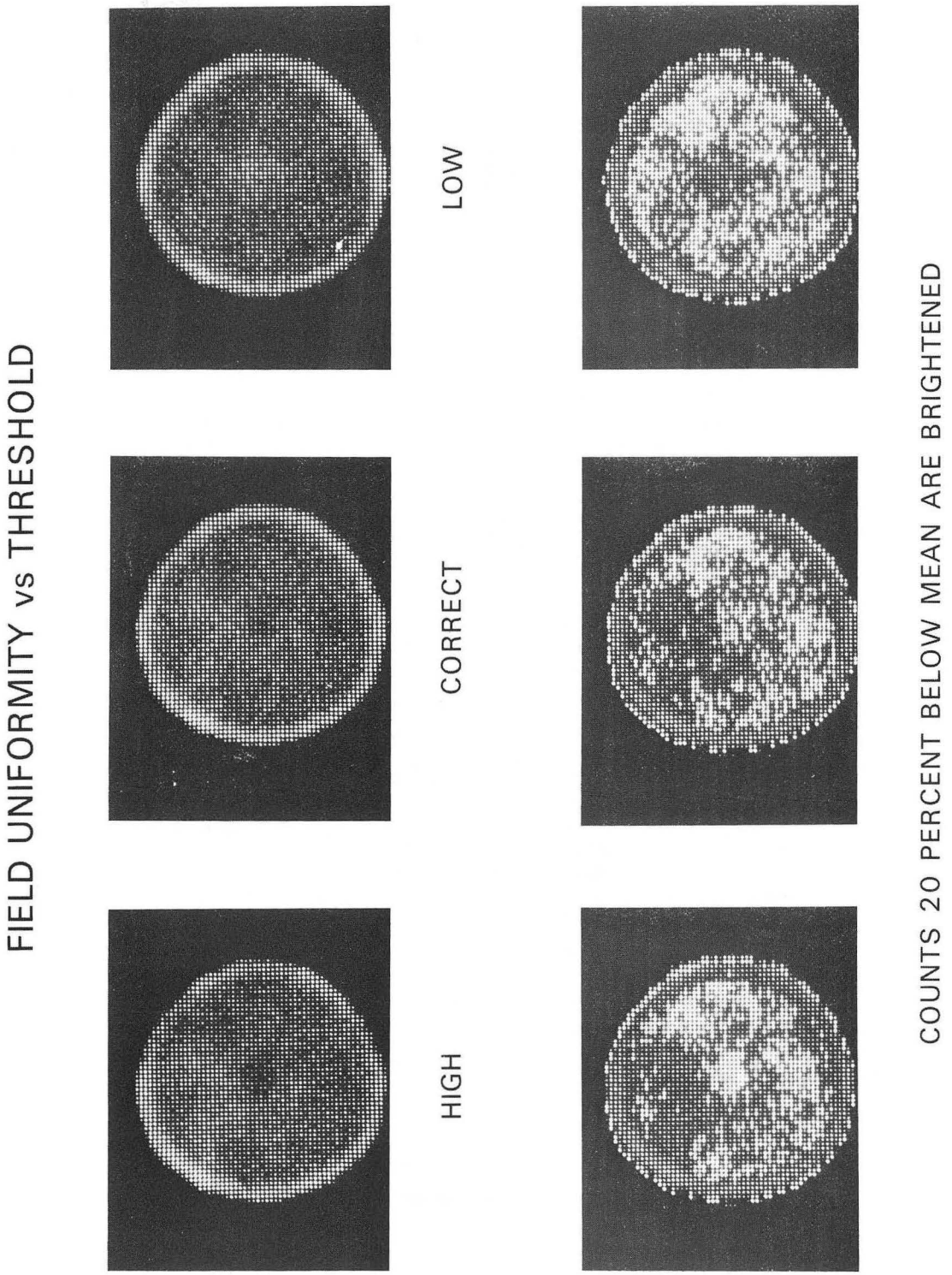

Fig. 12. Illustration of the change in camera response from symmetrical to asymmetrical placement of the window around the photopeak.

system impulse response changes markedly with distance from the camera [37]. By analogy NASA would have the problem of imaging the back side and front side of the moon from one photograph. A second, and perhaps more serious problem, is the presence of nonadditive noise.

The presence of multiplicative or nonadditive noise leads to a fundamental problem in the use of image enhancement techniques employed in one-dimensional or two-dimensional data processing. For example, the Wiener filter approach [25] is based on optimizing signals in the presence of additive noise, and does not allow for nonadditive noise, which is the major noise contribution in nuclear medicine studies. This can be seen by noting in the derivation of the Wiener filter that the power spectrum of the image is given by

$$|\Phi(s) \cdot H(s) + N(s)|^2 \approx \Phi^2(s) \cdot H^2(s) + N^2(s) \tag{7}$$

where $\Phi(s)$ is the object spectrum, $H(s)$ is the transfer function, and $N(s)$ is the noise spectrum. Note that the cross terms $\Phi(s)H(s) \times N(s)$ and $N(s) \times \Phi(s)H(s)$ are not present because correlation between object and noise is assumed to be negligible, which is not true in nuclear medicine imagery. The Wiener filter is derived from the criterion of minimum mean square error between the object and the ideal image, which is an estimate that is a linear functional of the image data [25, 38]:

$$Z(s) = \frac{H^*(s)}{H^2(s) + N^2(s)/\Phi^2(s)} . \tag{8}$$

The filter function $Z(s)$ multiplies the Fourier transform of the image and the inverse transform of this product gives the best restoration of the object projection.

$$V(\vec{r}) = \mathcal{F}^{-1}\{Z(s) \times \mathcal{F}(I(\vec{r}))\} \tag{9}$$

where $\mathcal{F}$ denotes the Fourier transform and $\mathcal{F}^{-1}$ the inverse Fourier transform. The Wiener filter approach is limited insofar as the nonadditive noise is present. This approach becomes more appropriate to use where statistics are good. The digital implementation of this filter involves five two-dimensional Fourier transforms. This is not an unreasonable task for a small machine because two-dimensional (64×64) transforms can be done in less than three minutes on 16-bit machines with 1 μsec cycle time. One frequently sees or hears the argument that the ideal image can be extracted from the observed image $I(x, y, z)$ by deconvolution of the object function, $V(x, y, z)$, from the system impulse response since

$$I(x', y', z') = \int\int\int V(x, y, z)\, h(x'-x,\ y'-y,\ z'-z)\, dx\, dy\, dz \tag{10}$$

and the impulse response $h(x, y, z)$ can be determined. From the Fourier convolution theorem we have

$$V(x, y, z) = \mathcal{F}^{-1}[\mathcal{F}(V)] = \mathcal{F}^{-1}\left[\frac{\mathcal{F}(I)}{\mathcal{F}(h)}\right]. \tag{11}$$

However, as has been recognized [25, 39, 40], the transfer function $\mathcal{F}(h)$ will not coincide with the zeroes of the Fourier transform of a noisy image. In the frequency region where $\mathcal{F}(h)$ is less than the noise N(s), the inverse filter approach leads to large amplifications of the noise. Thus in straightforward deconvolution techniques there is a high probability that finite numbers will be divided by very small numbers or zeroes at numerous places in the spatial frequency domain. This leads to images further from the object than the original, as shown by Fig. 13.

3.3 Three-dimensional reconstructions

An important goal of nuclear medicine quantitation is the determination of the three-dimensional distribution of compounds and their changes with time. Analogous goals in electron microscopy, radiology, and radioastronomy have led to problems whose mathematical physics are similar. There are four computer-method categories of image reconstruction from multiple views:

1) Back projection or direct methods [41, 42],
2) Back projection from modified projected densities [43, 44],
3) Iterative arithmetic reconstruction [45, 46, 47],
4) Fourier reconstruction techniques [48, 49].

All of these methods assume that the image is representative of a projection of the object–which is true under certain conditions in microscopy and nuclear medicine. Unfortunately, both noise and varying response function with distance between camera and image leave nuclear medicine with the hardest problems. Nevertheless, with a resolution length of 1/30th the field of view, reconstructions can be made by using large or small computer systems. The digital system at Donner Laboratory has the flexibility to implement the four classes of reconstruction programs.

3.4 Practical approaches to image restoration and enhancement

As elegant as the linear systems analysis approach is, unfortunately it is severely limited by nonadditive noise. Nevertheless, using some concepts from linear systems theory, practical and valid approaches are available for the enhancement and restoration of the ideal image. These can be divided into two categories: (1) smoothing for noise filtering, and (2) compensation for degradation due to the impulse response of the imaging system.

First some spatial averaging is necessary in order to simulate a continuous distribution from which the discrete counts arise. This procedure is justified from the fact that the distribution in the body is continuous, and smoothing operations will not prejudice the data if a smoothing function is varied to take into account the statistical significance of the data. Fixed area smoothing such as 9-point two-dimensional averages, weighted or unweighted, will result in superfluous blurring because the intensity in the areas of low counts and, therefore, low statistical significance will be increased to the same degree as the intensity in areas of high count; therefore, high statistical significance is lowered. An appropriate technique is the variable spatial averaging of Pizer and Veeter [50] and Tauxe [51, 52]. Variable smoothing is achieved by varying the radius of the smoothing domain inversely with the measured intensity. Thus areas of high count rate where the statistical significance is great might

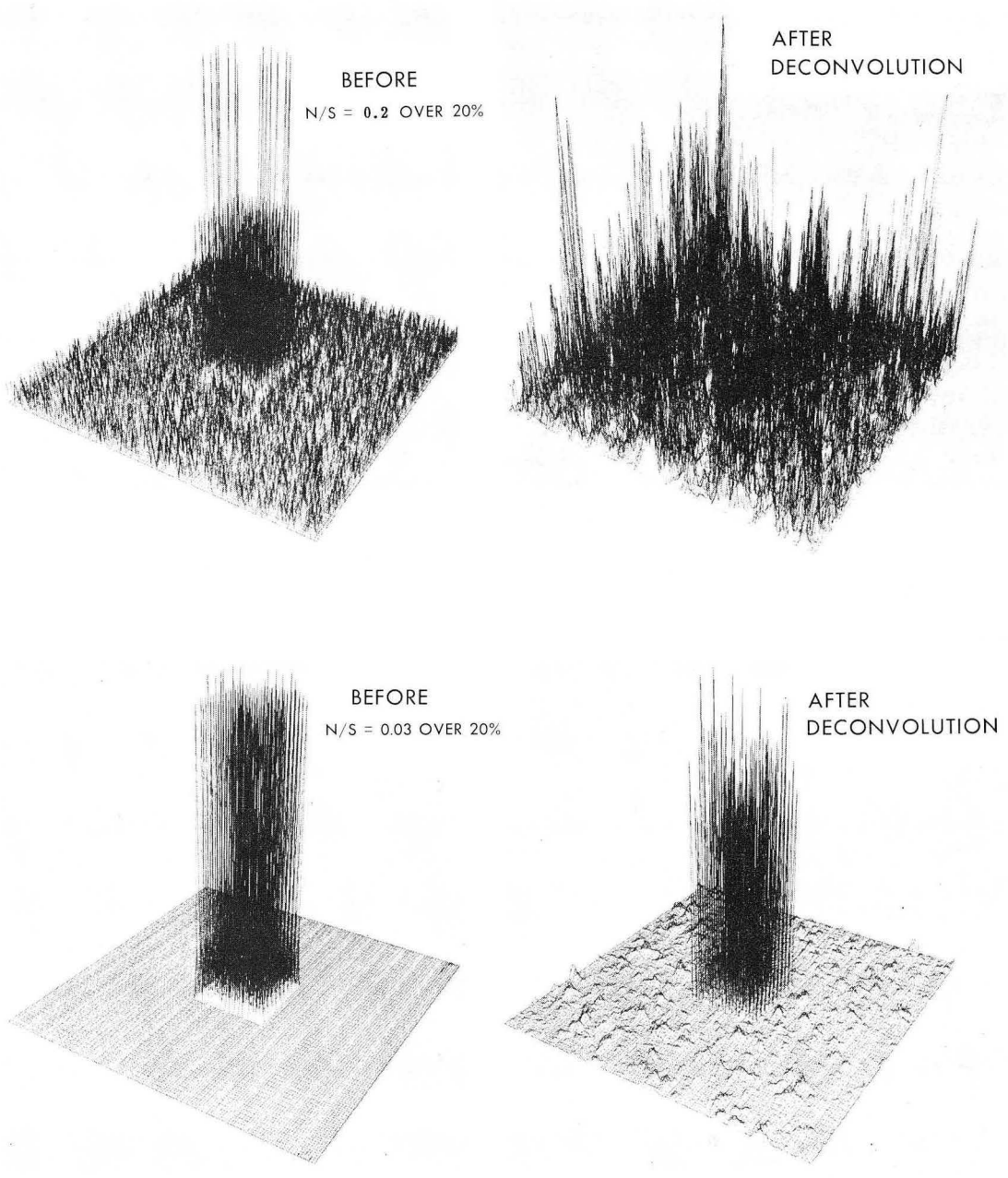

Fig. 13. Attempt at deconvolution of the impulse response from a noisy image frequently leads to a worse image than the original.

require a 5-point smoothing function, whereas in areas of low count rate the 9-point smoothing is appropriate.

The degradation of the image caused by the instrument impulse response or point spread function can be compensated for by indirect or iterative deconvolution suggested by Skarsgard, Johns, and Green [53] and implemented by Iinuma and Nagai [54] and Nagai, Iinuma and Koda [55]. The interative approach requires knowledge of the impulse response at a given distance from the camera. We can calculate

$$I_n = I_{n-1} + I_{(x,y)} - \mathcal{F}^{-1}\{\mathcal{F}(I_{n-1}) \cdot \mathcal{F}(h)\} \qquad (12)$$

where $I_{(n)}$ is the nth iteration on the image intensities and $\mathcal{F}$ denotes a Fourier transform for the rapid implementation of the approach of Iinuma and Nagai [54]. The best restoration occurs after a few iterations, and before the absolute value of the difference between the observed pixel (picture element) and the calculated pixel is equal to or greater than the standard deviation of the observed pixel count. For each pixel

$$\left|I(x,y) - I_n(x,y)\right| \leq \sqrt{I(x,y)}. \qquad (13)$$

Squaring both sides and summing over all pixels, we find

$$\sum_{j=1}^{N} \frac{[I^j - I^j{}_n]^2}{I^j} \leq N. \qquad (14)$$

One can implement the impulse response deconvolution by iterative approximation by noting that equation [12] can be rewritten as

$$I_n(x) = \mathcal{F}^{-1}\{\phi(s)\, H_n(s)\} \qquad (15)$$

where $H_n(s) = \{1 - \mathcal{F}[h(x)]\}^n + \{1 - \mathcal{F}h(x)\}^{n-1} \cdots \{\mathcal{F}h(x)\}$. (16)

Thus the iteration can be seen as merely the multiplication of the spatial frequency distribution of the image $\phi(s)$ by a frequency correction factor [56]. Thus for a particular collimator, energy, energy window, and distance to the patient we can compute a set of $\{H_n(s)\}$ (n is the number of iterations) and for a given image calculate a few $I_n(x)$, say for n = 3, n = 10, and n = 13. The convergence criterion of Eq. (14) can be used to stop the iteration and control the smoothing. The rate of convergence is related to the counting statistics, thus to the type of smoothing to be used for selecting the best image. The ideal image is calculated from taking the inverse transform of the product $\phi(s)\, H_n(s)$ of the observed image spectrum and the correction factor. At present each transform takes 3 minutes in the small computer, but we can have this speed at 15 sec with some additional hardware. Nevertheless the convenience and present speed of the two-dimensional Fourier transform program allow the researcher and curious clinician to explore iterative approximation deconvolution and other methods of image filtering. Restoration of images by means of

iterative approximation depends on the type of smoothing used [56], and the optimum filter has not been determined. It is reasonable to expect that a nonlinear filtering technique such as the Pizer-Vetter variable spatial averaging or the technique of maximizing entropy [25, 57] will give smoothing which least biases the data. Both methods are based on the criterion of minimizing prejudice by maximizing entropy [58].

Smoothing by 9-point averaging and enhancement control of the contrast (gamma), brightness, and dynamic range of the CRT display in most cases give adequate images for appropriate communication of the diagnosis to the referring clinician or patient chart. Figure 14 demonstrates this point. Defocusing is an effective means of filtering the 64×64 raster (Fig. 14).

Another approach which is intuitively appealing and gives direct results under the dynamic control of the operator is known as dot shifting [59, 60]. Dot shifting is simply an attempt to remove the smearing effect of a point spread function by moving counts from an element of low statistical significance toward regions of higher count density. The rationale for this technique is based on the fact that the high count regions are the most probable origin for outlying counts. An edge enhancement is effected. The absolute value of the two-dimensional spatial derivative also gives an edge enhancement. Another interesting technique of edge enhancement involves subtraction of the ratio of the Compton window counts to the photopeak window counts from the photopeak image [61]. This is a simple task if the computer system is designed to handle more than one energy or isotope at one time.

The search for optimum frequency filters [62-67] involves evaluating images formed after selective attenuation of the image spatial frequencies. The filters involve a two-dimensional mask which diminishes or enhances the selected spatial frequencies in a way based on the system MTF or Wiener filter derivation; or in an adaptive way based on the power spectrum of the image. Many filters have realizable real space analogs and Wiener filters can be simulated by convolution with a real space 5×5 weighted averaging function [66].

The field of image enhancement in nuclear medicine has not been hampered by lack of ideas--it has been hampered by lack of computing ability. Practical derivation of appropriate filters can be made by determining the set of frequency filters $\mathcal{F}(h)$ which will give the best reconstruction of a phantom (object) from the scintigraphic data (image). Thus we seek

$$\mathcal{F}_z(h) = \frac{\mathcal{F}(\text{image})}{\mathcal{F}(\text{object})}$$

for a particular organ, distance between the organ and imaging system z, collimator, and energy. With adequate computing ability now available one can not only determine the optimum filter but can store these filters for image enhancement in subsequent patient studies. We expect to speed up our three-minute two-dimensional Fourier transform program by a factor of 10 and give the nuclear medicine clinician or researcher the ability to do spatial frequency filtering without recourse to large computers.

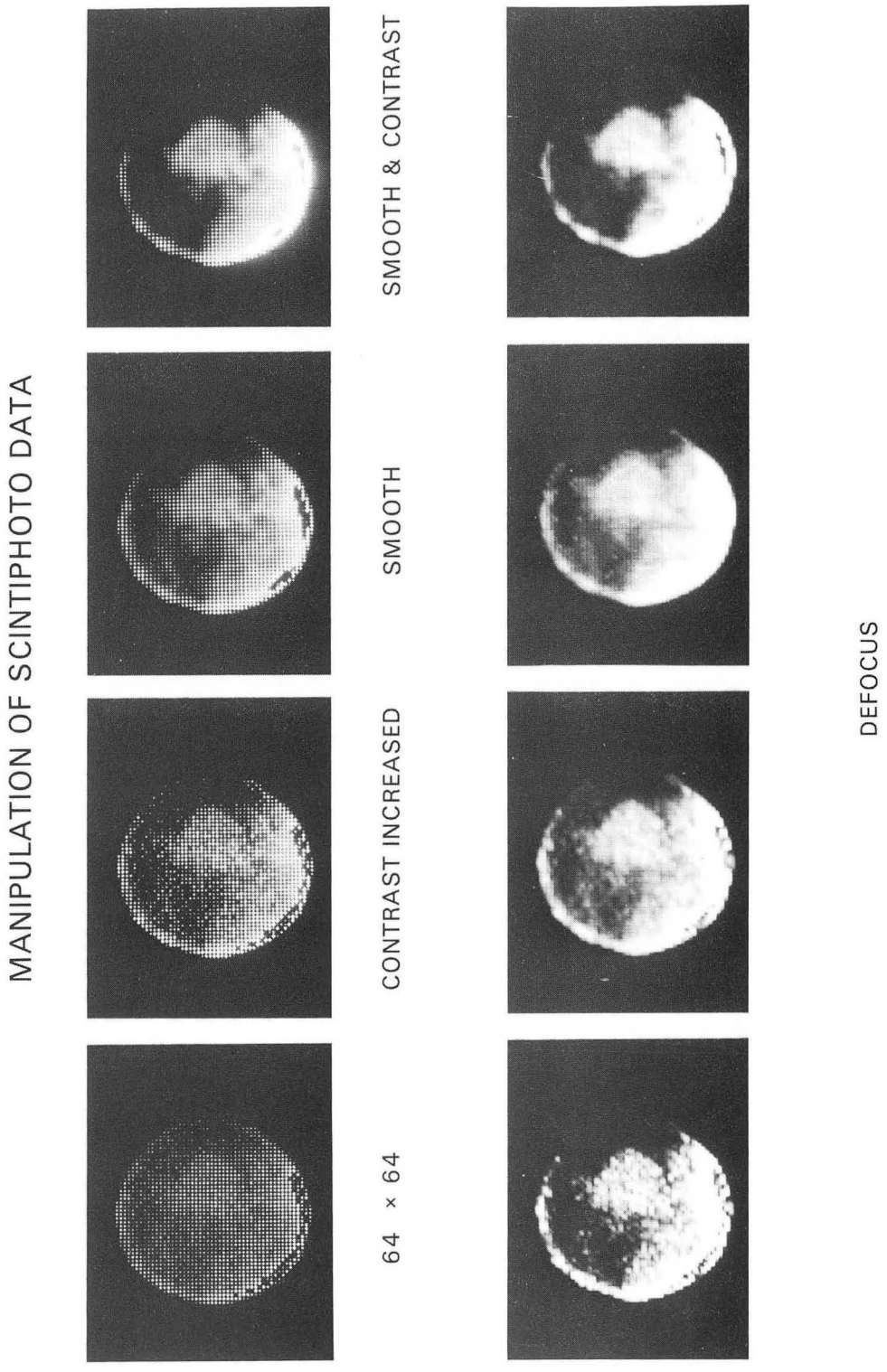

Fig. 14. Example of methods of contrast enhancement and smoothing easily implemented by control of the display module.

Another use of the two-dimensional Fourier transform is in motion extraction by the powerful holographic image deblurring method first described by Stroke and Zech [68]. This approach has not been tried, and is perhaps more cumbersone than the digital technique of Oppenheim [69]. Integral transforms can also be used to transform a Fresnel or Bessel zone plate image to real space, thus obviating the inconveniences and expense of optical reconstruction.

3.5 Time functions

Once we have restored the image to the best representation of the object, we can proceed with the tasks of generating functional images depicting organ uptake and washout, images of dual isotope distribution, transmission-emission images in multiple colors, and time functions (time-activity curves). Speed and convenient display are the objectives of the system design for manipulation of data frames or time functions extracted from these images. An example from a pancreas study will give a measure of the speed and convenience. The teletype keys under "AREA OPERATIONS" (Fig. 7) are used for the area-of-interest operations. Five areas for the pancreas-liver study were delineated by light pen in 2 minutes (Fig. 15). The time functions (time-activity curves) are created by a stroke of the "create" key, and counts vs frame curves containing 80 points each were generated simultaneously in 40 sec. Four curves can be displayed at one time, and hard-copy other than CRT photographs can be produced by using the TTY for three time functions simultaneously, as illustrated in Fig. 4. The following manipulations of TF's are implemented on the HP-5407 system:

1. Addition, subtraction, multiplication, and division of TF by scalers.

2. Addition, subtraction, multiplication, and division of one TF by another (Fig. 16).

3. Differentiation and integration between time or spatial coordinate limits.

4. Modification by logarithmic, exponential, square root, and trigonometric operators.

5. Dead-time correction.

6. Convolution of time function (TF) with smoothing operator.

7. Fourier transform of a time function (or spatial function) [22].

8. Normalization to unit area or volume.

9. Retrospective gating.

10. Fit of a time function to exponential decay.

11. Extraction of the impulse response, given the input and output functions (4 minutes).

12. TTY plot of three TF's simultaneously.

Methionine uptake curves

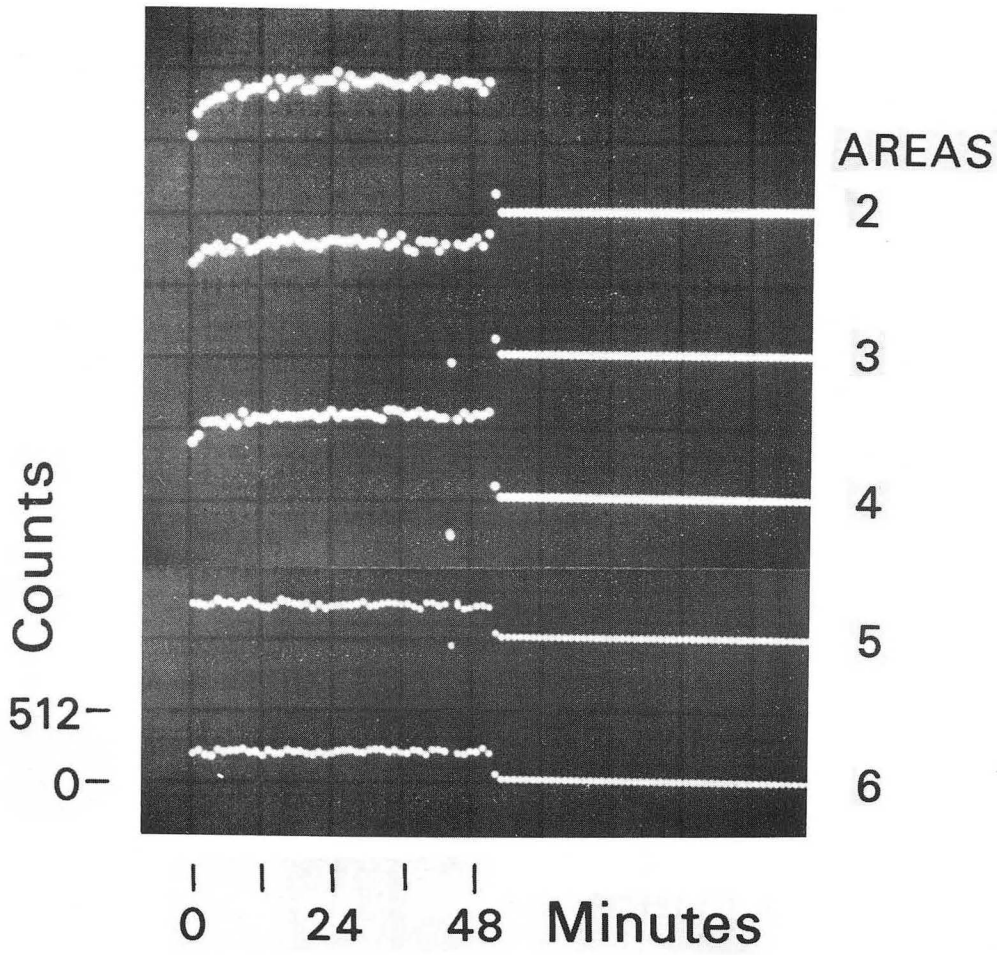

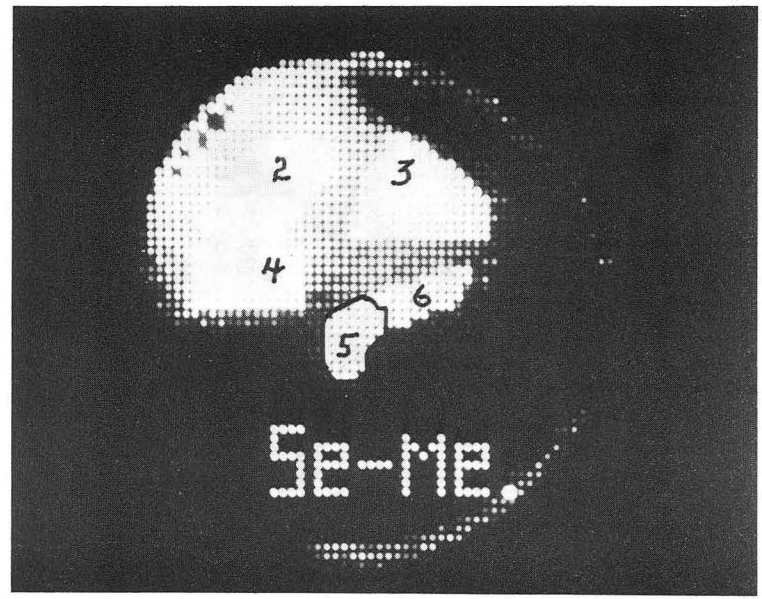

Areas for integration selected by light pen

Fig. 15. Pancreas study using 200 μCi ^{75}Se-methionine which shows rate of uptake in three areas over the liver and the head and tail of the pancreas.

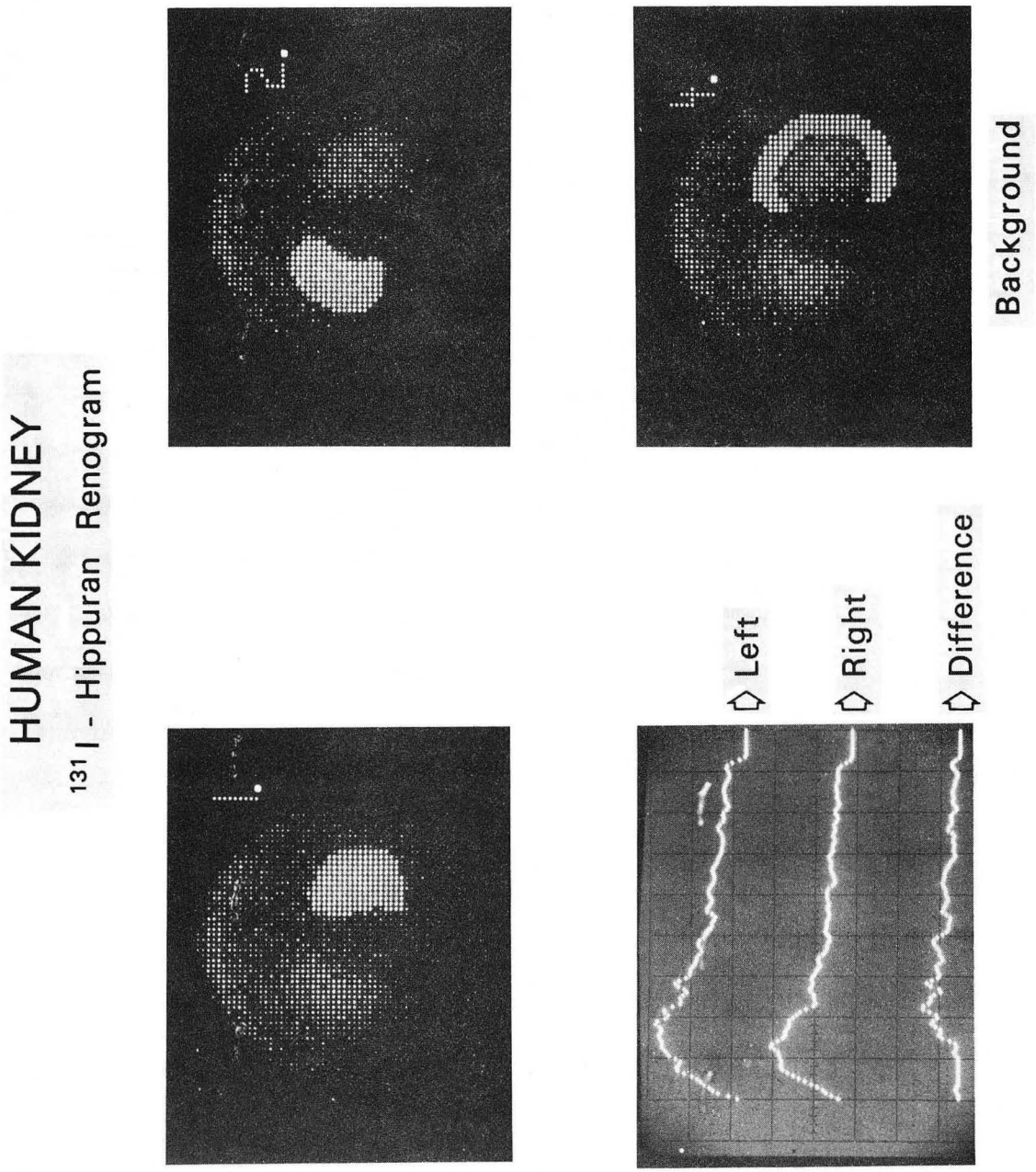

Fig. 16. Example of rapid subtraction of one time function (renogram) from another.

The ability to do operation No. 1 implies the capability for the other operations; for example, restrospective gating is done by smoothing and differentiation of a time-activity curve such as that of Fig. 17. This operation is based on the ability to subtract one point of a TF from an adjacent datum.

The extraction of impulse response is done by calculating the inverse Fourier transform of the ratio of the Fourier transform of the output to the Fourier transform of the input. In theory the response of the system, be it systemic circulation or lungs, is invariant with respect to the input function. Thus if we have a known input function and a known output, we can determine the transfer function and, therefore, the distribution of transit times of the system. This is a practical application of linear systems theory and can be accomplished if the statistics are good.

The system response h(t) is the inverse transform of the ratio of the Fourier transform of the output time function to the input time function:

$$h(t) = \mathcal{F}^{-1}\left[\frac{\mathcal{F}(B)}{\mathcal{F}(A)}\right]. \tag{17}$$

But the mean transit time is $\overline{t} = \int th(t)dt$. This transform approach [25, 70, 71] has been examined from the standpoint of determination of the number of compartments and their importance [72]. We are interested in an approach which takes into account noise and seeks a solution which minimizes the mean-squared value of noise [25]. In this case the system response is determined from the cross power spectrum of the output and input S_{AB} and the power spectrum of the input

$$\mathcal{F}h(t) = \frac{S_{AB}}{S_{AA}} = \frac{\mathcal{F}\{R_{AB}\}}{\mathcal{F}\{R_{AA}\}} \tag{18}$$

where R_{AB} and R_{AA} are the cross correlation of input and output and the autocorrelation of the input functions, respectively. Solution for the impulse response by using Eq. (17) takes 4 min, using the FFT (about 0.5 min for 128-point transform [22]; however, a hard-wired fast Fourier transform can complete the three transforms in less than 1 sec [22]. Programs for manipulating TF's can be written in BASIC, FORTRAN, ALGOL, or machine language. The BASIC programs call in TF's by a subroutine CALL READT (..., ..., ...) and CALL WRITT(..., ..., ...). Simple subtraction of one entire time function from another requires less than 0.5 sec with results displayed on CRT or hard-copy via TTY. Subtraction of one renagraph from another by this technique is shown in Fig. 16.

The purpose of rapid manipulation of time functions is to give the clinician and researcher the following capabilities with little more than a stroke of a key.

(a) Heart dynamic functions: The cardiopulmonary system can be evaluated by high speed digital systems and simple arithmetic manipulations without any off-line processing. The cardiac parameters that can be readily evaluated include:

(1) Systemic circulation time, obtained by measuring the time interval from the peak of the right ventricle dilution curve to the peak of the recirculation on the same curve [73].

(2) Cardiac output

$$C.O. = \frac{\text{blood vol.} \times \text{count rate at equilibrium}}{A} .$$

The denominator represents the area under the dilution curve obtained by extrapolating the washout to the zero or background intercept. The blood volume is determined as the ratio of the total counts injected over the activity per volume ascertained by venous blood activity measurements and extrapolation to zero time to account for the few percent loss of, say, technetium-albumin from the blood pool.

An alternative procedure for cardiac output is to calculate

$$C.O. = \frac{\text{blood volume}}{\text{systemic circulation time}} .$$

Blood volume and systemic circulation are available every time ^{99m}Tc-albumin study is done.

(3) Left to right cardiac shunt detection [74, 75, 76]

(4) Intracardiac circulation times [77, 78, 79, 80]

(5) Left ventricular wall movement and calculation of ejection fractions [21, 29, 81, 82, 83, 84]

A large literature exists on the extraction of end-systole and end-diastole volume information from biplane or single view angiography using contrast agents [85, 86]. Most of these approaches can be duplicated by isotopes which pass through or remain in the blood pool. The single-plane topologic approach can be used along with a modified Simpson's rule to calculate these important volumes.

$$V = \frac{\pi t}{3}\left[\frac{1}{4}\left(d_0^2 + d_{2n}^2\right) + \sum_i d_i^2 + \frac{1}{2}\sum_j d_j^2\right] \qquad (19)$$

where t is the thickness of an even number of strips placed perpendicular to the axis of the ventricle outline, d_i denotes the odd diameters, and d_j denotes the even diameters surrounding the strips. Essential to this approach is high speed and high spatial resolution (128×128), because the calculation rests on accurate edge determination. Analysis of 32×32 or 40×40 images must rely on quantity of isotope during phases of the cardiac cycle and subtraction of background activity, which is less satisfactory than the topological approach which does not require background subtraction. Retrospective gating such as illustrated in Fig. 17 involves use of the time function for determination of the frames of maxima and minima. These frames are summed to give images of end-diastole and end-systole shown in Fig. 17 and Fig. 19.

(6) Qualitative assessment of cardiac function pioneered by Kriss

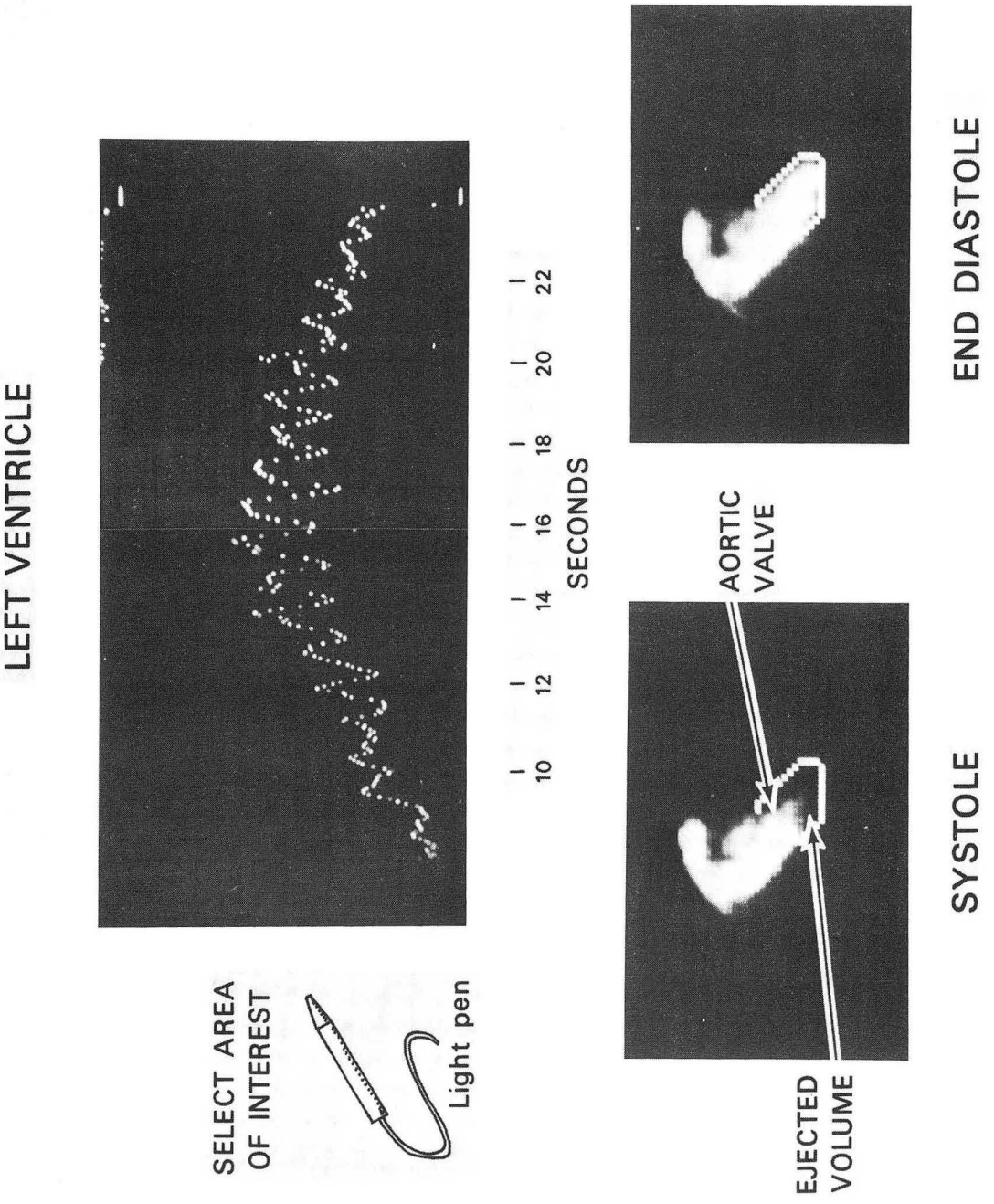

Fig. 17. Example of retrospective gating wherein the time-activity curve was generated at 50 msec intervals by using an area over the left ventricle four count integration. The sum of the frames at maximum activity gives an image of end-diastole and the frames at minimum activity give end-systole.

and co-workers [88] on analog systems can be made using this digital system, if adequate spatial resolution for display is available. Assessment of the relations of myocardium to heart silhouette and to left ventricle is shown in Fig. 18, and the time relations of heart circulation are shown in Fig. 19 [89].

(7) Time function patterns of disease: A screening procedure for valvular disease proposed by Goldberg and coworkers [90, 91] involves calculating the ratio of FWHM of left atrium to FWHM of left ventricle uptake-washout curve after normalization to the FWHM of the input function (right ventricle). The qualitative evaluation of uptake-washout curve patterns promises to give us diagnostic radioangiograms similar to EKG's, if the acquisition system does not introduce errors (Fig. 4).

(b) Renography and computer-assisted blood background subtraction techniques [92-99].

(c) Lung perfusion: ventilation and xenon washout studies [16, 100-105].

(d) Cerebral blood flow symmetry [14, 20, 106-109].

(e) Thyroid uptake function [110-112].

(f) Gall bladder—labeled dye excretion studies [113].

(g) Myocardial flow studies [114, 115].

(h) Liver dynamic function [116, 117].

(i) Decay correction (flourine-18, oxygen-15, nitrogen-13).

(j) Cross talk correction; e.g., removal of contributed activity from overlapping regions such as pulmonary artery contribution to aortic output curve or Compton addition from dual isotope studies.

3.6 Manipulations of images

Most of the arithmetic operations available for the scaler time functions are also available for whole images (64×64 frames). These include: addition, subtraction, multiplication, division of frames by other frames or by scalers. For example the operation:

(a) $3 \times (^{72}\text{Se-methionine})$ FRAME No. 4 - (^{99m}Tc-sulfur colloid) FRAME No. 5 into FRAME No. 10.

(b) Smooth FRAME No. 10.

Can be done by executing the following:

F1 * 3 → F4

F4 - F5 → F10

Smooth F10.

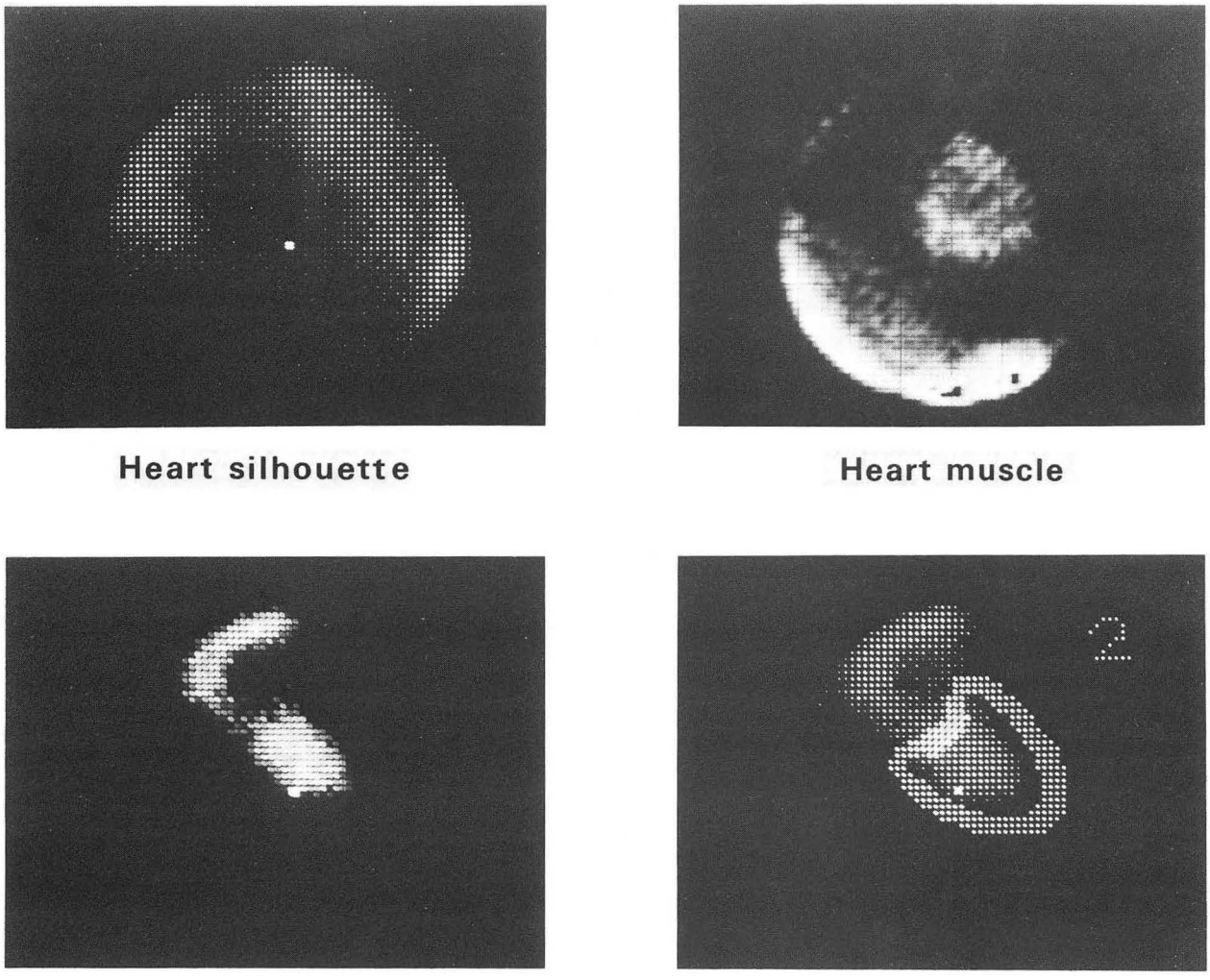

Fig. 18. Combination of transmission and emission imaging using ^{129}Cs and ^{99m}Tc which demonstrates relationships of myocardial uptake to intracardiac chamber and heart silhouette.

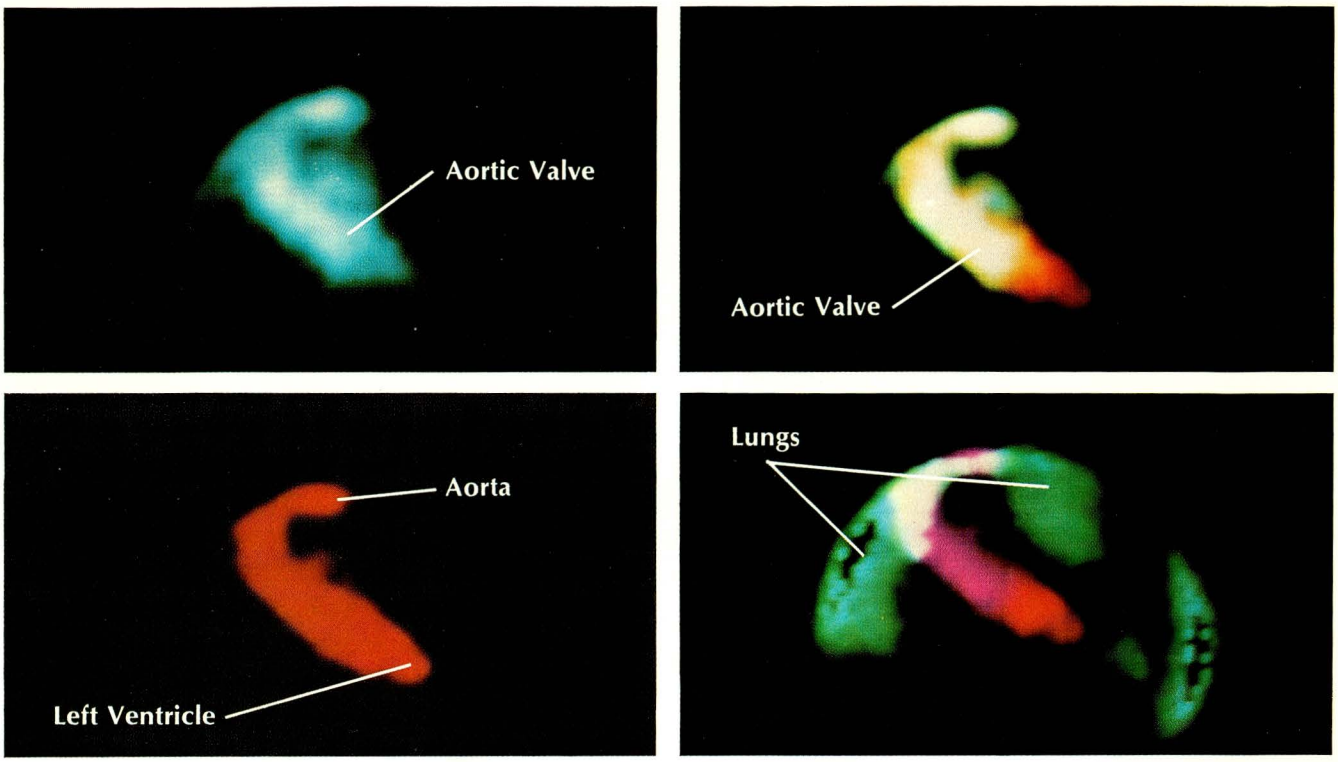

End systole and end diastole can be visualized by color coding the moments when maximum and minimum activity appears in left ventricle after injection of a tracer. In these scintigrams by Dr. Thomas F. Budinger of the Donner Laboratory, end systole is at upper left, end diastole at lower left. When these two images are superimposed (upper right), ejected volume is seen as red. Combining this image with simultaneous transmission image shows relationship to lungs and silhouettes heart (lower right).

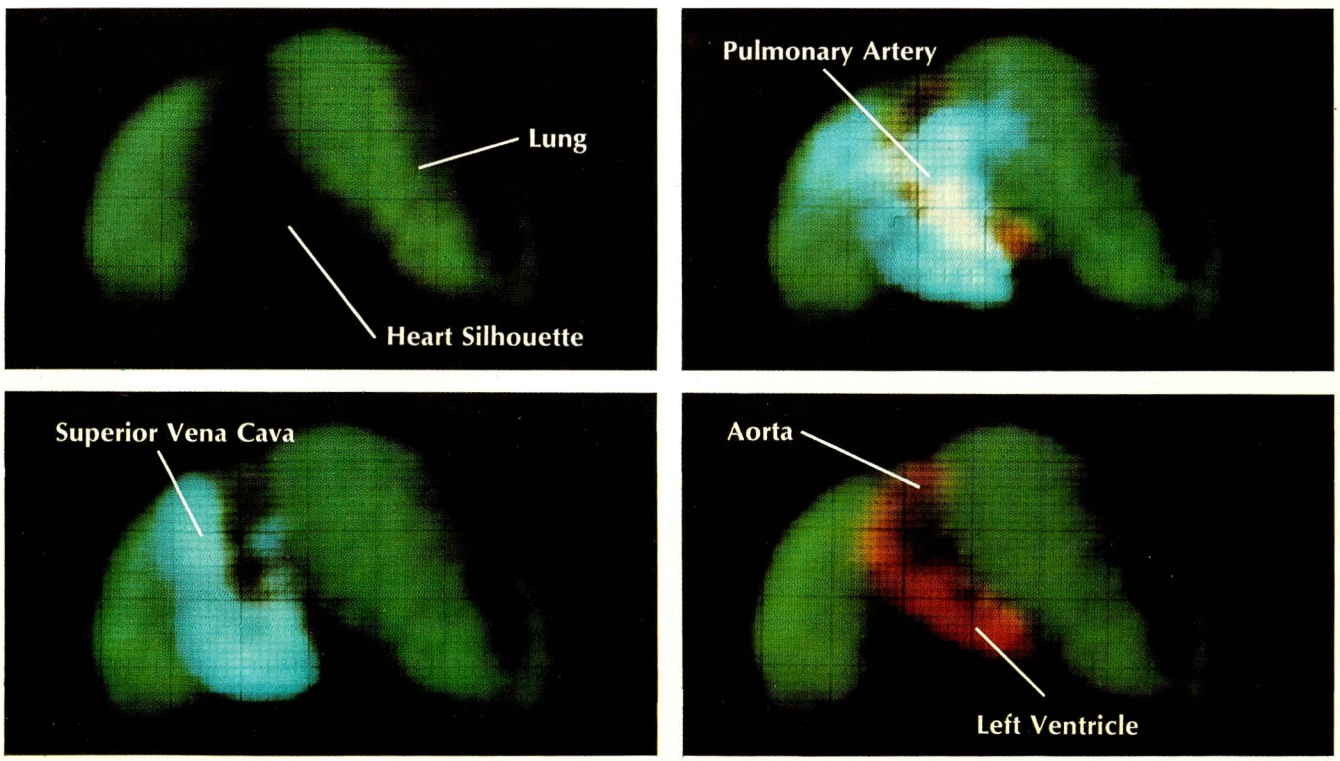

Color coding of time intervals demonstrates flow of isotope through heart and lungs (also by Dr. Budinger). At upper left is transmission image of lungs; below it, ^{99m}Tc-albumin bolus enters right heart at 6-8 seconds following antecubital injection and starts out through pulmonary artery. At upper right, flow into pulmonary vasculature is seen 8-10 seconds after injection. Lower right, between 12-14 seconds, bolus has returned from the lungs and is in the left ventricle and ascending aorta.

Reprinted from Hospital Practice, September, 1972

The time to complete this operation is 12 sec, because that is the time needed to type in the commands. The results of this operation are shown in Fig. 20. This procedure of extracting an image using dual isotopes [118, 119] has had good results, particularly for pancreas studies [120-124]. Extracting a ^{67}Ga tumor uptake from a ^{198}Au liver has also proved of value [125].

A functional image [126-128] such as a rate image involves subtracting a frame at t_{n-1} from a frame at t_n. The result is displayed as a functional rate image. The functional image depicting washout has been advocated by MacIntyre and Inkley [129] for lung studies, and J. Kriss for myocardial flow studies [personal communication]. This is an image of magnitudes of the rate constants λ_{ij} for each pixel. A measure of specific topographic function of any organ is the rate of clearance of some substance. This rate can be a measure of flow, metabolism, or ventilation. Flow is derived by multiplying the fraction cleared per unit time by the amount present. The fraction cleared is usually validly approximated by the rate constant λ in the single exponential decay. Determination of λ is made for each pixel of each successive frame. By the least-squares criterion, λ_{ij} is determined for pixel ij by assuming the observed counts A(t) are given by $A_0 e^{-\lambda t}$:

$$\lambda_{ij} = \frac{\Sigma t \, \Sigma \ln A(t) - N \Sigma t \ln A(t)}{N \Sigma t^2 - [\Sigma t]^2} . \tag{20}$$

Unfortunately this solution employs an improper weighting resulting from treatment of $\ln A(t) = \ln A_0 - \lambda t$ as the linear function $Y = Bx$. In effect we have minimized $\Sigma[\ln A_0 - \lambda t - \ln \bar{A}(t)]^2$. A valid approach which minimizes $\Sigma[A_0 e^{-\lambda t} - \bar{A}(t)]^2$ and assumes a weighting by the square root of the observed count value A(t) leads to a solution

$$\lambda = \frac{\Sigma A(t) \, t \, \Sigma[A(t) \times \ln A(t)] - \Sigma t \, A(t) \, \ln A(t) \, \Sigma A(t)}{\Sigma A(t) \, \Sigma[t^2 \, A(t)] - [\Sigma t \, A(t)]^2} . \tag{21}$$

The product of λ and the amount present gives a flow image.

Ratio and difference images can be produced for different energies, times, or isotopes. The keyboard instructions for these operations consist of: F1/F2 > F3 for ratios, and F1 - F2 > F3 for difference images. The time is less than 1 sec for the calculations on 64 × 64 frames.

3.6.1 Statistical significance image

The clinician needs some measure of the statistical significance of both static and functional images. This can be done by deriving images whose intensities reflect the significance of some computed parameter such as the rate constant λ, or as multiples of the standard deviations of the difference between one pixel and eight surrounding pixels [4]. Values of multiples of the standard deviation of differences can be calculated from:

$$n = \frac{|A_i - A_o|}{\sqrt{A_i + A_o}} . \tag{22}$$

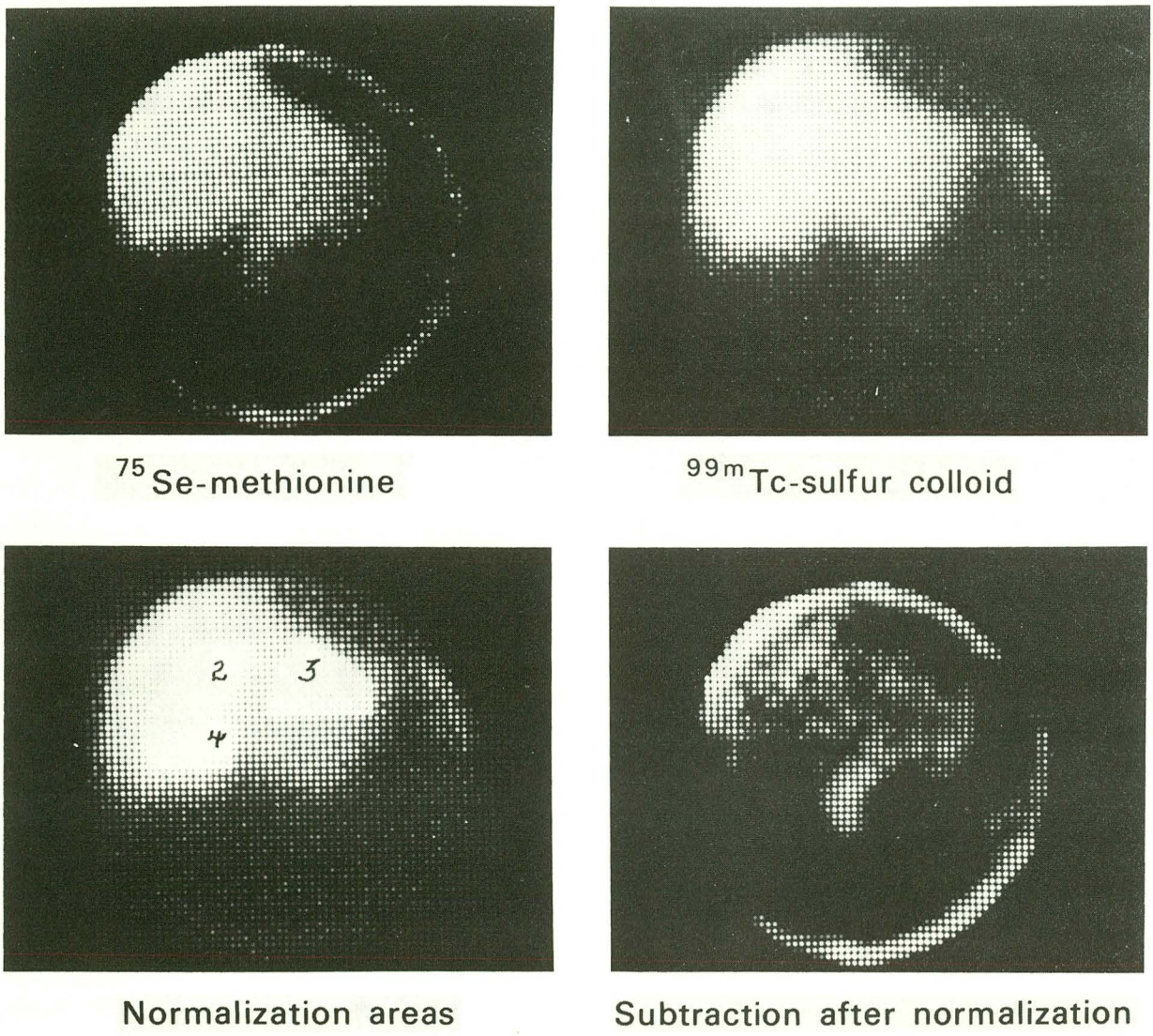

Fig. 20. Pancreas extraction by subtraction of the ^{99m}Tc-sulfur colloid image from the ^{75}Se-methionine image after normalizing one to the other, using three regions over the liver.

The usefulness of these significance images has not yet been evaluated. Another image of potential usefulness is the gradient image wherein the magnitude of the spatial gradient is calculated and images are presented for magnitudes greater than some selectable constant

$$\left|\frac{\partial}{\partial x} + \frac{\partial}{\partial y}\right| \geq K .$$

3.6.2 Uses of color to depict function and pathology

Arguments for or against color coding of intensities continue unresolved between those who use color and those who claim black and white gives them the reference point for their diagnosis and all the available information. We do not use color for intensity coding as has been done through both analog and digital systems [130-134]. Color has great usefulness if used to code time for demonstrating dynamic function as shown in Fig. 19, for transmission-emission images (Figs. 18, 21, 22) and differential uptake in dual isotope studies (Fig. 21). We see this as an effective method of relating the basis for our diagnostic conclusions to the clinician. Clearly an added dimension can be included in one image if color is used to code time, energy, or isotope. Additional studies for which multicolor images efficiently convey the basis for diagnostic impressions include: emission-transmission studies for subphrenic abscess; emission-transmission studies for pericardial effusion using ^{129}Cs or ^{43}K myocardial images and lung transmission images, dual isotope studies of liver and thyroid using technetium and gallium or selenomethionine, dual isotope studies of the liver using ^{67}Ga and ^{198}Au colloid, dual isotope renograms, and color coding of time changes in ventilation-perfusion ratios for clinical follow of patients with pulmonary disease, as has been suggested by Burdine and co-workers[102]. Color can be generated by insertion of Wratten filters between the CRT and camera, or by more sophisticated (and more costly) techniques using a three-gun color CRT and solid state memories. We use Polaroid 180 film and Wratten filters with a P-31 phosphor (38 μsec). The P-4 (white) is a better phosphor, and can be substituted by a modular replacement on our display scope.

4. WHOLE-BODY SCANNER DIGITAL SYSTEM

4.1 Interface to the digital computer

A rapid 64-detector scanner operates by moving the patient over the 2.5 cm × 2.5 cm NaI(Tl) crystal detector array [135]. Pulse-height selection is used to separate pulses caused by ^{241}Am 60 keV photons and by pulses from the administered isotope. Scan durations can vary from 0.75 min to hours. This scanner has been interfaced to the computer system in a fashion which allows simultaneous acquisition of up to four photon energies (Fig. 2). Thus we have the capability to quantitate the distribution of isotopes in the whole body in a single scan, and to observe the time vs. activity relations for various organs over hours or days. The detector consists of 4 rows of 16 detectors, each row offset diagonally from the others. The table position, detector identification, and isotope are encoded by a hardware device which presents the computer with a 16-bit word:

15 14 13 12 11	10 9 8	7 6	5 4	3 2 1 0
not used	bed position	isotope	column	detector row

A 2048-word buffer is filled every eight table positions (4 isotopes × 8 table positions × 64 detectors = 2048 words). As this buffer is being filled, another buffer is dumped onto the raw data disc (Fig. 6). After accumulation, these data are framed into 6 frames of 64×64, which takes less than 10 seconds. The frames are created from the raw data, and stored in the frame file in a fashion similar to scintillation camera frames. Since we recognize four separate isotopes, each scan can involve twenty-four 4K frames. These frames are displayed in 64×64 or 64×128 format, and a light pen is used to delineate areas (e.g., kidney, bone, heart) for integration.

The system sofeware for the scintillation camera is available for manipulation of the whole-body scanner data. In addition, we have a special detector sensitivity correction program and the ability to offset one accumulated scan relative to another scan, in order to register the patient position from hour to hour or day to day. Figure 22 is an example of the whole-body scan showing the body silhouette in red (^{241}Am transmission) and the distribution of ^{99m}Tc-EHDP at 18 hours after injection of 10 mCi in a patient with metastatic bone tumors. The potentials of this system for quantitating the long-term kinetics of electrolytes and compounds is shown by the change in potassium distribution with time after injection of ^{43}K intravenously (Fig. 23).

4.2 Quantitative whole-body scanning

Quantitative measures of the changes in the spatial and temporal distribution of isotopes and radiopharmaceuticals are vital to the analysis of the metabolic fate of injected or ingested substances as well as to the precise calculations of radiation dose. The problems of precise regional quantitation have been analyzed since 1937 when Robley Evans [136] successfully estimated the amount of radioactivity in radium dial painters. The following variables are involved:

1) Patient thickness [136, 137],

2) Source thickness and homogeneity [137, 138],

3) Photon attenuation coefficient,

4) Geometry effect,

5) Source position.

For the Donner whole-body scanner, we assume negligible geometry effect, because the crystals are collimated. However, the 64 detectors are not collimated by an exact parallel hole-straight bore array. Thus there will be some slight geometry effect which we have neglected in our analysis. If the quantitation is done on an organ region basis rather than an element by element basis using both supine and prone scans (conjugate scanning), then the geometry effect should be negligible. Source thickness was taken into account by Genna [138] and source homogeneity

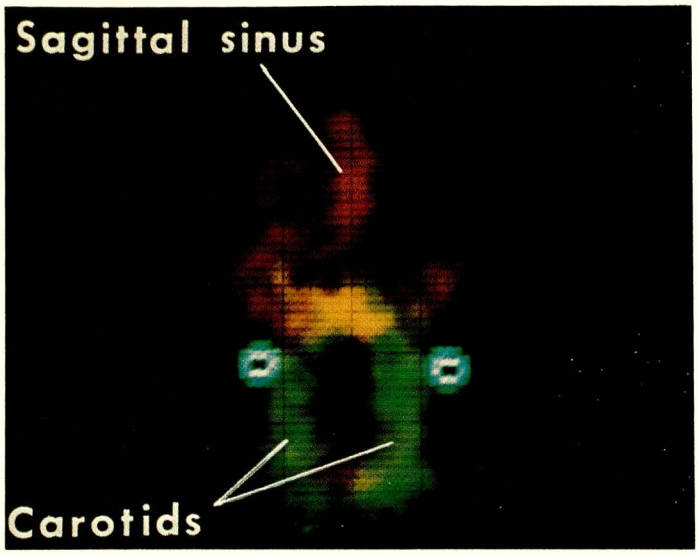

Dynamic brain scan. Green is early carotid phase, red is venous phase. Blue denotes sources over eyes.

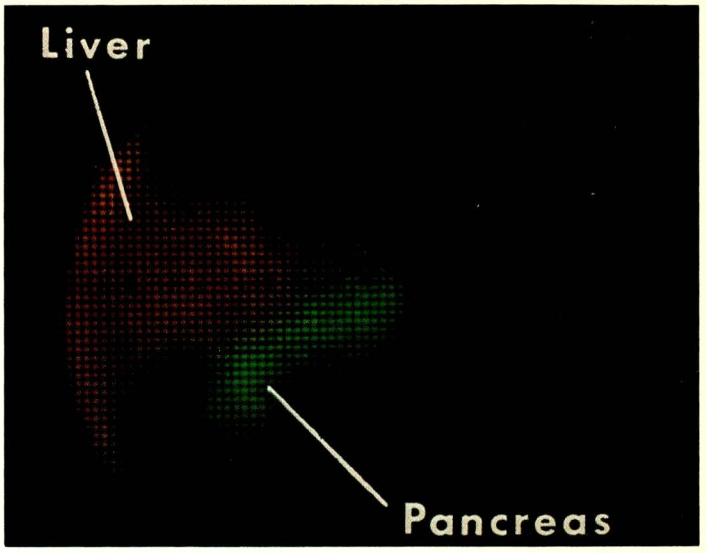

^{75}Se-methionine pancreas image (green) extracted by removing normalized ^{99m}Tc sulfur colloid image (red).

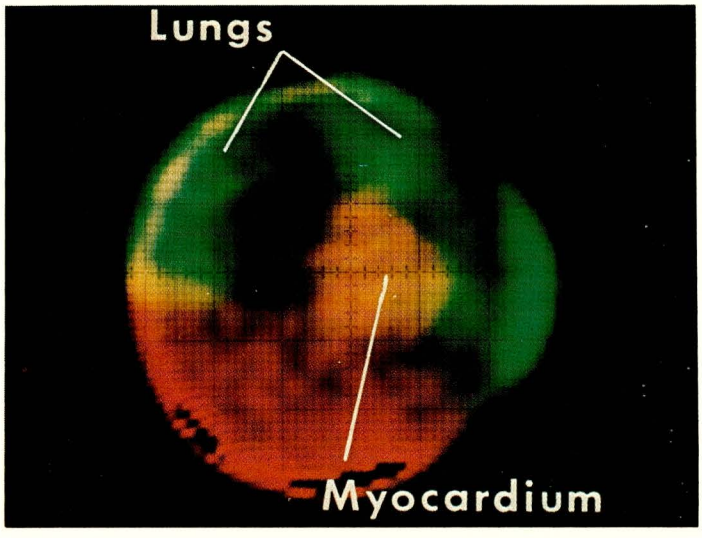

Human normal myocardium uptake of ^{43}K(yellow) with liver and GI tract (red).

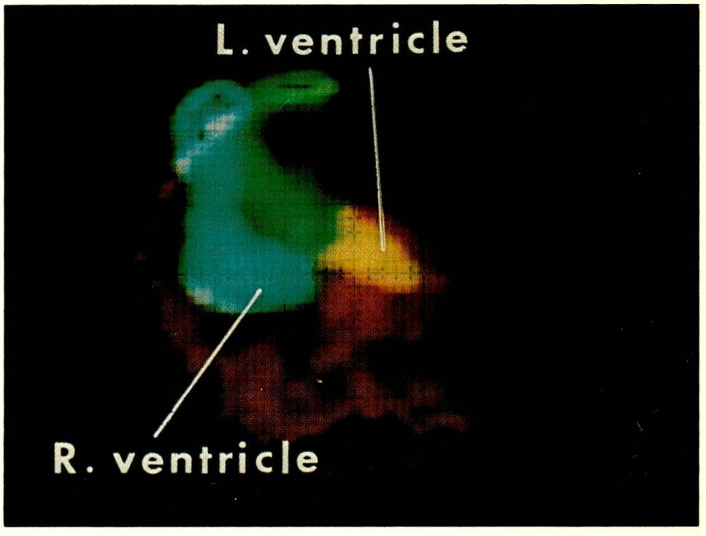

Relationships of intracavitary blood volumes to myocardium (red).

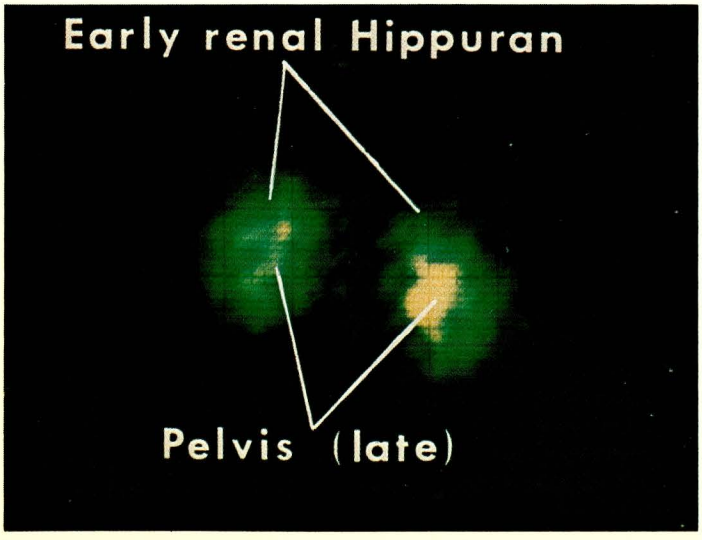

Symmetrical flow coding by color, showing ^{131}I-hippuran flow from cortex (green) to (yellow).

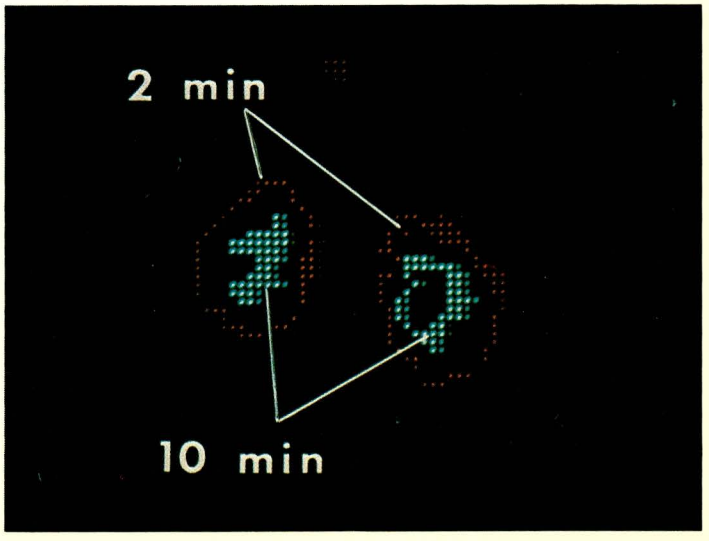

Use of fixed window to depict change in activity with time.

WHOLE BODY SCAN (64 x 384)

^{99m}Tc-EHDP

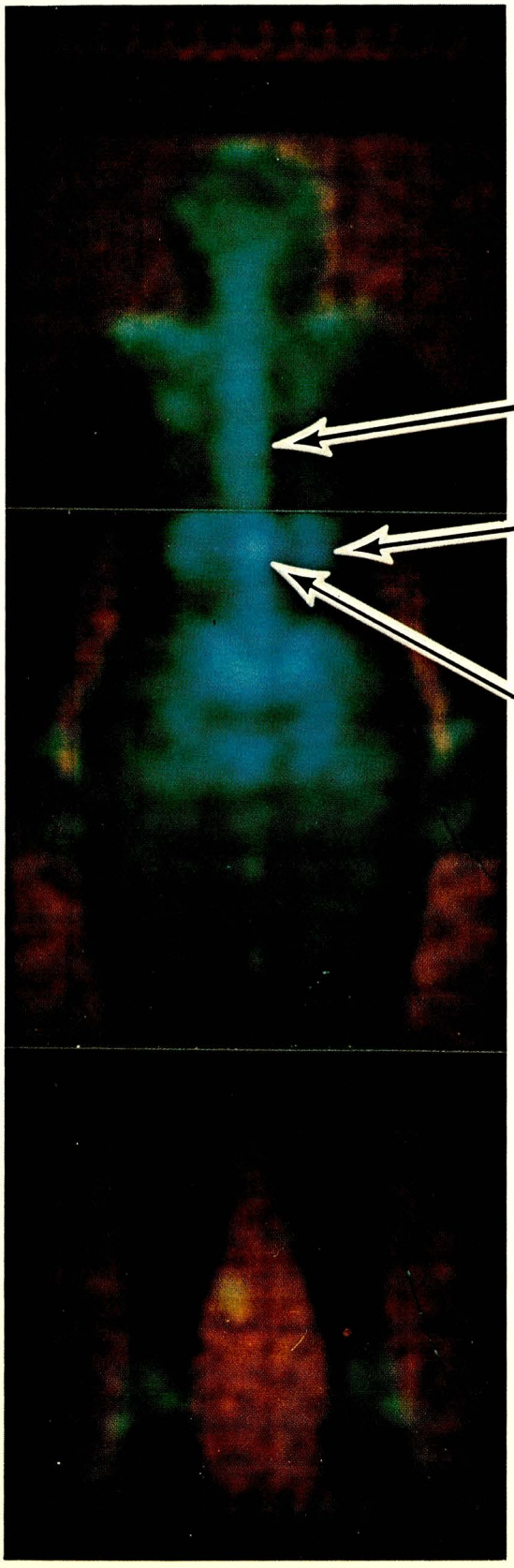

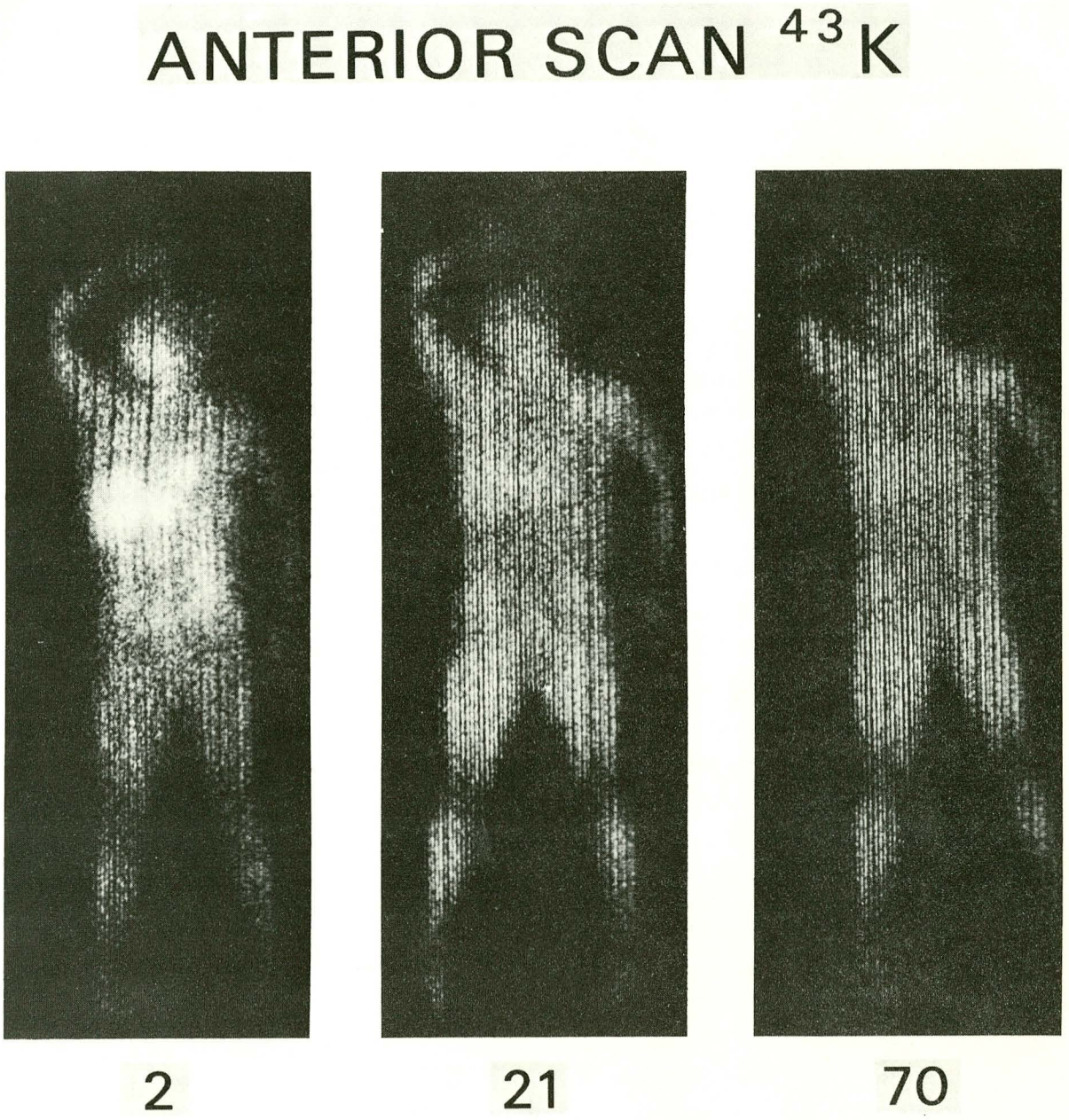

Fig. 23. Whole-body distribution of potassium over a three-day period after 500 μCi of ^{43}K i. v.

was included in the analysis by Sorenson [137].

The analysis applicable to the Donner whole-body scanner starts by assuming we can measure the body thickness at each point, T_{ij}, in a 64×384 array by scanning the patient under a source of ^{241}Am, ^{99m}Tc, or ^{57}Co. The measured attenuation of photons by the presence of the body for photons > 100 keV gives a good measure of effective body thickness:

$$T_{ij} = \frac{\ln (Nb/Na)}{\mu}$$

where Nb and Na are the counts before and after the patient is positioned and μ is the linear attenuation coefficient. During a supine scan, the isotope emission counts, dAs, contributed by a small thickness increment, dx, of the body is related to the activity from that portion of the body as $A^o_{ij}\, dx/T_{ij} \cdot f$ where $f\ (>0)$ is the linear fraction of the body thickness wherein the isotope is distributed. The emission counts are also related to the attenuation coefficient and the depth of the increment in the body, thus--

$$dA^s_{ij} = C \cdot A^o_{ij}/fT_{ij}\ (e^{-\mu x} dx) \tag{23}$$

where C is a sensitivity and calibration factor. We integrate this over the body thickness to:

$$A^s_{ij} = \frac{C \cdot A^o_{ij}\, e^{-\mu m} \sinh(f\mu T_{ij}/2)}{f\,\mu T_{ij}/2} \tag{24}$$

where m is the mean source depth which will cancel when the prone scan is included. (Note: $\sinh Z = \frac{1}{2}(e^Z - e^{-Z})$)
We get a similar expression for the prone scan:

$$A^p_{ij} = \frac{C \cdot A^o_{ij}\, e^{-\mu(T-m)} \sinh(f\mu T_{ij}/2)}{f\,\mu T_{ij}/2} \tag{25}$$

The activity A^o_{ij} is determined from the geometric mean $\sqrt{A^s A^p}$ and a multiplication factor to account for the thickness T_{ij} at each pixel:

$$A^o_{ij} = \frac{(A^p_{ij}\, A^s_{ij})^{1/2}\, e^{\mu T/2}\, f\mu T_{ij}}{2\, C \sinh(f\mu T_{ij}/2)} \tag{26}$$

Both T and μ can be determined. An estimate of $f = 2/3$ has been shown by Sorenson [137] to lead to errors less than ±10% using supine-prone scans.

Because of bone density is 2 times soft tissue density the contribution from attenuation through the body is not accurately given by a constant attenuation coefficient, μ; however, for photons above ~100 keV we

do not expect this to lead to significant errors.

Quantitation of the amount of activity in a specific organ will be more accurate if we integrate the counts over the region of the organ delineated by light pen before performing the calculation of Eq. (26). From our preliminary studies we expect an absolute accuracy of ± 10% and a precision of ± 3% .

4.3 Organ function by whole body clearance rate

In addition to the direct quantitation discussed above, the whole-body scanner provides a unique opportunity to determine organ clearance of substances which are removed from the blood by only one organ. It is assumed that the rate of excretion or disappearance of a substance is proportional to the concentration of that substance in the plasma:

$$- \frac{d A_t(t)}{dt} = \lambda A_p(t) \qquad (27)$$

where $-dA_t/dt$ is the rate of whole body disappearance and $A_p(t)$ is the amount in the plasma. To relate Eq. (27) to clearance rate, we note $A_p = C_p \times V_p$, where C_p and V_p are, respectively, plasma concentration and plasma volume. Thus the volume clearance rate, C_v

$$C_v(t) = - \left(\frac{dA_t(t)}{dt}\right) / C_p(t) \{\text{ml sec}^{-1}\} \qquad (28)$$

Thus we can determine the instantaneous extraction rate of a particular organ by measuring the rate of change of the substance in the body and the plasma concentration. The derivative $dA_t(t)/dt$ is an excretion rate from the entire body. Usually the clearance function being evaluated such as glomerular filtration rate or liver extraction is estimated by the accumulation into the organ of interest, and not extraction out of the rest of the body. The conventional clearance rate method is limted by the degree to which the extracted material returns to the plasma or moves out of the organ, such as into the tubules in the case of kidneys, and into the biliary tree in the case of the liver. The apparent organ extraction, $+ dA_o(t)/dt$, is proportional not only to the clearance, but also the rate of removal from the organ of interest. Thus, if the relative change in whole-body counts is known, and from this we exclude the contribution from the organ of interest and compartment to which the cleared substance is excreted, we have a simple measure of function in so far as the assumption of Eq. (27) is correct. The whole-body scanner quantitation system allows one to readily implement these ideas because the change in counts over the whole body, exclusive of the organ of interest, can be determined by subtracting the organ contribution using a light pen for removing regional counts. This is an improvement over shielded whole-body counter methods [139, 140].

5. SUMMARY

Nuclear medicine diagnostic techniques have as their main advantage the ability to delineate organ function in health and disease. Both digital and analog data handling systems have enabled us to measure blood flow through organs and metabolic fates of radiopharmaceuticals. However, without data acquisition devices which have speed and spatial resolution capabilities similar to that obtainable by the imaging devices, the prospects of implementing dynamic function studies in clinical practice are limited. Thus over the last few years a nuclear medicine data handling system has evolved to overcome the limitations of other systems, and the frustrations of researchers and clinicians who have pioneered this field for the last eight years (most are cited in the references).

The system acquires data at rates of 82 kHx (128×128) in list mode or 300 kHz (64×64) in histogram mode with 200 MHz ADC's which have a pulse pair resolution of 3 μsec. The 16-bit word of the Hewlett-Packard 2100A computer is configured to handle dual isotope studies with physiological triggers. Images (128×128) can be stored at a rate of 100 sec^{-1} in list mode. This system can carry up to 160 images and 16 time-activity curves at any one time for manipulation and display. The programs available range from field uniformity correction to two-dimensional (64×64) Fourier transforms. Both time-activity curves and images can be manipulated rapidly by system's programs for addition, subtraction, multiplication, and division. In addition, these data are available for BASIC, FORTRAN, ALGOL, or machine language programs. Convenience, flexibility, and speed are the result of a fast computer (980 nsec cycle time) and two moving head discs.

This system has been used to do brain, heart, kidney, pancreas, and bone studies using the Anger camera. Body distribution studies using the Anger whole-body scanner, involves digitizing six 4K frames (64×384) with 4 energies in order to do transmission-emission imaging and quantitative patient scanning.

ACKNOWLEDGMENTS

The system specifications and desired characteristics, most of which have now been implemented at Donner and are available to other medical scientists, were based on the objectives of doing justice to the Anger scintillation camera and whole-body scanner. Hal Anger, Frank Upham, and Victor Elisher gave constructive criticism of the design criteria as they evolved over the past few years. William Hogan, Grant Gullberg and Victor Elisher provided invaluable computational assistance for work performed on computing machines at the Lawrence Berkeley Laboratory in order to test our ideas and those of other authors. The majority of the software for the Hewlett-Packard 5407 system was written by John Harpootlian, and the system for the whole-body scanner was done by Paul Banchero and Jean C. Roy. James Doub and Edward Muns were the Hewlett-Packard engineering leaders with whom the Donner researchers interacted during the development of this system. Don Wyman and Ron Liddell were instrumental in keeping this system on the air during its clinical trials over the past six months. Finally, I wish to acknowledge the invaluable assistance of Jack H. Klinger whose enthusiasm and tenacity resulted in the evolution of the system not only appropriate for our research needs, but ideal for the day-to-day use of the nuclear medicine clinician. The color reproduction of Fig. 19 was kindly denoted by Hospital Practice.

I am indebted to Drs. James Born, James McRae, and John Lawrence for their continuing encouragement.

This work was supported by the U. S. Atomic Energy Commission.

REFERENCES

[1] BROWN, D. W., "Digital computer analysis and display of the radionuclide scan", J. Nucl. Med. 5 (1964) 802.

[2] MYERS, J. J., KENNY, P. J., LAUGHLIN, J. S., "Quantitative analysis of data from scintillation camera", Nucleonics 24 (1966), 58.

[3] SMITH, E. M., BRILL, A. B., "Progress with computers in nuclear medicine", Nucleonics 25 (1968) 64.

[4] BENUA, R. S., WEBER, D. A., KENNY, P. J., LAUGHLIN, J. S., "Digital scanning compared with photoscanning in liver examination", J. Nucl. Med. 9 (1968) 135.

[5] KUHL, D. E., EDWARDS, R. Q., "Perforated tape recorder for digital scan data store", J. Nucl. Med. 7 (1966) 269.

[6] HEISS, W-D., PROSENZ, P., ROSZUCZKY, A., TSCHABITSCHER, H., Verwendung von Gamma-Kamera und Vielkanalspeicher zur Messung der gesamten und regionalen Hirndurchblutung", Nuclearmedizin 7 (1968) 297.

[7] LAUGHLIN, J. S., WEBER, D. A., BENUA, R. S., KENNY, P. J., RITTER, F., "Quantitative storage, analysis and display in digital scanning", in Fundamental Problems in Scanning (GOTTSCHALK, A., BECK, R., Eds.) C. C. Thomas, Springfield, Ill. (1968) 267.

[8] MacINTYRE, W J., CHRISTIE, J. H., CURTIS, G. S., "Three-dimensional computer read-out of radioisotope scan data", Radiology 90 (1968) 22.

[9] BENDER, M. A., MOUSSA-MAHMOUD, L., BLAU, M., "Quantitative radiography with the digital autofluoroscope", Medical Radioisotope Scintigraphy 2 (Proc. Symp. Salzburg, 1968) IAEA, Vienna (1969) 57.

[10] GORIS, M., De ROO, M. J. K., VANDERSCHUEREN, G., "An approach to a storage and data handling procedure in static and dynamic scintigraphy", J. Belge de Radiol. 52 (1969) 168.

[11] MAYNARD, C. D., COWAN, R. J., ADDARIS D., "Use of cerebral radioisotope arteriography and the 1600 channel analyzer in the diagnosis of brain lesions", J. Nucl. Med. 10 (1969) 358.

[12] NATARAJAN, T. K., WAGNER, H. N., JR., "A new image display and analysis system (IDA) for radionuclide imaging", Radiology 93 (1969) 823.

[13] WINKLER, C., KNOPP, R., SCHULTE, P., "Computer-Nephrographie ein Programm zur Automatischen Auswentung und Befundausgabe von Isotopenephrogrammen", Nuclearmedizin 8 (1969) 154.

[14] POTCHEN, E. J., BENTLEY, R., GERTH, W., HILL, R. L., DAVIS, D. O., "A means for the scintigraphic imaging of regional brain dynamics. Regional cerebral blood flow and regional cerebral blood volume", pp. 577-583 in Medical Radioisotope Scintigraphy 2 (Proc. Symp. Salzburg, 1968) IAEA, Vienna (1969).

[15] ASHBURN, W. L., MOSER, K. M., GUISAN, M., "Digital and analog processing of Anger camera data with a dedicated computer-controlled system", J. Nucl. Med. 11 (1970) 680.

[16] BELL, R. L., DeNARDO, G. L., "Enhanced scintigraphic information display using computer-generated ratio techniques", J. Nucl. Med. 11 (1970) 655.

[17] BRUNO, F. P., BROOKEMAN, V. A., WILLIAMS, C. M., "A digital computer data acquisition display and analysis system for the gamma camera", Radiology 96 (1970) 658.

[18] BRILL, A. B., ERICKSON, J. J., LINDAHL, C. E., "Digital systems for data acquisition and storage", pp. 339-379 in Quantitative Organ Visualization in Nuclear Medicine (KENNY, P. J., SMITH, E. M., Eds.) University of Miami Press, Coral Gables, Florida (1971).

[19] COX, J. R., JR., HILL, R. L., III, "Design considerations for interfacing computers to gamma-ray cameras", pp. 465-480 in Quantitative Organ Visualization in Nuclear Medicine (KENNY, P. J., SMITH, E. M., Eds.), University of Miami Press, Coral Gables, Florida (1971).

[20] HEISS, W-D., PROSENZ, P., ROSZUCZKY, A., "Technical considerations in the use of a gamma camera 1600-channel analyzer system for the measurement of regional cerebral blood flow", J. Nucl. Med. 13 (1972) 534.

[21] WEBER, P. M., DOS REMEDIOS, L. V., JASKO, I. A., "Quantitative radioisotopic angiocardiography" (in press, J. Nucl. Med.).

[22] BUDINGER, T. F., "Rapid manipulation and display of counts vs. time curves by hardware and software", Proc. 2nd Symp. Sharing of Computer Programs and Technology in Nuclear Medicine (Oak Ridge, Tennessee, 1972) USAEC Rep. CONF-720430 (1972) 306.

[23] BERMAN, M., SHAHN, E., WEISS M. F., "The routine fitting of kinetic data to models: a mathematical formalism for digital computers", Biophys. J. 2 (1962) 275.

[24] LLAURADO, J. G., "Relationship between kinetics of inflow and outflow as the basis of a computer simulation for solving compartmental models: example of electrolyte transfers in cardiovascular tissues", in Dynamic Studies with Radioisotopes in Medicine (Proc. Symp. Rotterdam, 1970) IAEA, Vienna (1971) 13.

[25] BUDINGER, T. F., "Transfer function theory and image evaluation in biology: application in electron microscopy and nuclear medicine" (Ph. D. Thesis) Lawrence Berkeley Laboratory Rep. LBL-565 (1971).

[27] MANDEL, J., Statistical Analysis of Experimental Data, Wiley, New York (1964).

[28] ERICKSON, J. J., BRILL, A. B., "Quantitative approach to determination of minimum digital resolution in digitized camera images", J. Nucl. Med. 11 (1970) 317.

[29] VAN DYKE, D., ANGER, H. O., SULLIVAN, R. W., VETTER, W. R., YANO, Y., PARKER, H. G., "Cardiac evaluation from radioisotope dynamics", J. Nucl. Med. 13 (1972) 585.

[30] BITTER, F., BESCH, W., SCHÄFER, N., SIGMUND, E., "Integrierte Herz-Kreislaufanalyse mit Hilfe der quantitativen Funktionsszintigraphie", in Frontiers of Nuclear Medicine (HORST, W., Ed.), Springer-Verlag, Berlin (1971) 250.

[31] BUDINGER, T. F., YANO, Y., "Myocardial function evaluation by uptake of ^{129}Cs", J. Nucl. Med. 13 (1972) 417.

[32] WOLFF, J. R., "Calibration methods for scintillation camera systems", p. 229 in Quantitative Organ Visualization in Nuclear Medicine (KENNY, P. J., SMITH, E. M., Eds.) University of Miami Press, Coral Gables, Florida (1971).

[33] MORRISON, L. M., BRUNO, F. P., MAUDERLI, W., "Sources of gamma camera image inequalities", J. Nucl. Med. 12 (1971) 785.

[34] OBERHAUSEN, E., NEUMANN, K. J., SCHIFFLER, W., "Method for adjusting the Anger camera", Medical Radioisotope Scintigraphy I (Proc. Symp. Salzburg, 1968).

[35] SMITH, E. M., "On methods for normalizing the response of the Anger camera imaging system", pp. 261-277 in Quantitative Organ Visualization in Nuclear Medicine (KENNY, P. J., SMITH, E. M., Eds.) University of Miami Press, Coral Gables, Florida (1971).

[36] SPECTOR, S. S., BROOKEMAN, V. A., KYLSTRA, C D., DIAZ, N. J., "Analysis and correction of spatial distortions produced by the gamma camera", J. Nucl. Med. 13 (1972) 307.

[37] ZIMMERMAN, R. E., HOLMAN, B. L., "Modulation transfer function for the pho/gamma III and pho/gamma HP scintillation cameras using ^{99m}Tc and ^{133}Xe", J. Nucl. Med. 13 (1972) 481.

[38] WIENER, N., Extrapolation, Interpolation, and Smoothing of Stationary Time Series, Technology Press and Wiley, New York (1949).

[39] SKARSGARD, L. D., JOHNS, H. E., GREEN, L. E. S., "Iterative response correction for a scintillation spectrometer", Radiation Res. 14 (1961) 261.

[40] HALL, W. D., MASSEY, N. G., "Optical spatial filtering", pp. 619-659 in Quantitative Organ Visualization in Nuclear Medicine (KENNY, P. J., SMITH, E. M., Eds.) University of Miami Press, Coral Gables, Florida (1971).

[41] RAMACHANDRAN, G. N., LAKSHMINARAYANAN, A. V., Proc. Natl. Acad. Sci. Wash. 68 (1971) 2236.

[42] KUHL, D. E., EDWARDS, R. R., "Digital techniques for on-site scan data processing", in Fundamental Problems in Scanning (GOTTSCHALK, A., BECK, R., Eds.) C. C. Thomas, Springfield, Ill. (1968) 250.

[43] KUHL, D. E., EDWARDS, R. Q., RICCI, A. R., REIVICH, M., "Quantitative section scanning using orthogonal tangent correction", J. Nucl. Med. 13 (1972) 447.

[44] GILBERT, P. F. C., "The reconstruction of a three-dimensional structure from projections and its application to electron microscopy. I. Direct methods", Proc. Roy. Soc. London B182 (1972) 89.

[45] GILBERT, P., "Iterative methods for the three-dimensional reconstruction of an object from projections", J. Theor. Biol. 36 (1972) 105.

[46] GORDON, R., BENDER, R., HERMAN, G. T., "Algebraic reconstruction techniques (ART) for three-dimensional electron microscopy and x-ray photography", J. Theor. Biol. 29 (1970) 471.

[47] GOITEIN, M., "Three-dimensional density reconstruction from a series of two-dimensional projections", Nuclear Instruments and Methods 101 (1972) 509.

[48] CROWTHER, R. A., DeROSIER, D. J., KLUG, A., "The reconstruction of a three-dimensional structure from projections and its application to electron microscopy", Proc. Roy. Soc. London A317 (1970) 319.

[49] KLUG, A., CROWTHER, R. A., "Three-dimensional image reconstruction from the viewpoint of information theory", Nature 238 (1972) 435.

[50] PIZER, S. M., VETTER, H. G., "Processing radioisotope scans", J. Nucl. Med. 10 (1969) 150.

[51] TAUXE, W. N., "100-level smoothed scintiscans processed and produced by a digital computer", J. Nucl. Med. 9 (1968) 58.

[52] NAGAI, T., IINUMA, T. A., "A comparison of differential and integral scans", J. Nucl. Med. 9 (1968) 202.

[53] SKARSGARD, L. D., JOHNS, H. E., and GREEN, L. E. S., "Iterative response correction for a scintillation spectrometer", Radiation Res. 14 (1961) 261.

[54] IINUMA, T. A., and NAGAI, T., "Image restoration of radioisotope imaging systems", Phys. Med. Biol. 12 (1967) 501.

[55] NAGAI, T., IINUMA, T. A., and KODA, S., "Computer focusing for area scans", J. Nucl. Med. 9, (1968) 507.

[56] IINUMA, T. A., "Image enhancement by the iterative approximation method", p. 549 in Quantitative Organ Visualization in Nuclear Medicine" (KENNY, P. J., SMITH, E. M., Eds.) University of Miami Press, Coral Gables, Florida (1971).

[57] HALL, E. L., KRUGER, R. P., DWYER, S. J., III, HALL, D. L., McLAREN, R. W., LODICK, G. S., "A survey of processing and feature extraction techniques for radiographic images", IEEE Trans. Comput. 20 (1971) 1032.

[58] JAYNES E. T., "Information theory and statistical mechanics", Phys. Rev. 106 (1957) 620.

[59] PIZER, S. M., VETTER, H. G., "Processing radioisitope scans", J. Nucl. Med. 10 (1969) 150.

[60] PIZER, S. M. "Digital spatial filtering and its variations", p. 581 in Quantitative Organ Visualization in Nuclear Medicine (KENNY, P. J., SMITH, E. M., Eds.) University of Miami Press, Coral Gables, Florida (1971).

[61] ERICKSON, J. J., BRILL, A B., "Physical considerations for dual radionuclide imaging techniques", ibid. 777.

[62] BROWN, D. W., KIRCH, D. R., "Computer processing of radioisotope scans using the Fourier and other transformations", J. Nucl. Med. 12 (1971) 287.

[63] KIRCH, D. L., BROWN, D. W., "Recent advances in digital processing static and dynamic scintigraphic data", Proc. 2nd Symp. Sharing of Computer Programs and Technology in Nuclear Medicine (Oak Ridge, Tennessee, 1972), U.S.A.E.C. Rep. CONF-720430 (1972) 27.

[64] PISTOR, P., GEORGI, P., WALCH, G., "The Heidelberg scintigraphic image processing system", ibid. 411.

[65] BERCHE, C , TODD-POKROPEK, A E., Di PAOLA, R., "Preliminary results on the use of the Hadamard transform", ibid. 429.

[66] TODD-POKROPEK, A. E., "Problems of band pass filtering", p. 605 in Quantitative Organ Visualization in Nuclear Medicine", (KENNY, P. J., SMITH, E. M , Eds.) University of Miami Press, Coral Gables, Florida (1971).

[67] METZ, C. E., "A mathematical investigation of radioisotope scan image processing" (Ph. D. Thesis), University Microfilms, Ann Arbor, Michigan (1970).

[68] STROKE, G W., ZECH, R. G., "A posteriori image-correcting deconvolution by holographic Fourier-transform division", Physics Letters 25A (1967) 89.

[69] OPPENHEIM, B. E., "Method using digital computer for reducing respiratory artifact on liver scans made with a camera", J. Nucl. Med. 12 (1971) 625.

[70] BROWNELL, G. L., CALLAHAN, A. B., "Transform methods for tracer analysis", Ann. N. Y. Acad. Sci. 108 (1964) 1.

[71] BROWNELL, G. L., BERMAN, M., ROBERTSON, J. S., "Nomenclature for tracer kinetics", Int. J. Appl. Radia. Isotop. 19 (1968) 249.

[72] CALLAHAN, A. B., PIZER, S. M., "The applicability of Fourier transform analysis to biological compartmental models", p. 149 in Natural Automata and Useful Simulations (PATTEE, H. H., EDELSACK, E. A., FEIN, L., CALLAHAN, A. B., Eds.) Spartan Books, Washington (1966).

[73] LOKEN, M. K., PONTO, R. A., BACHE, R., BURCHELL, H., "Intravenous radioisotope angiography with computer processing of data", Am. J. Roent. Rad. Ther. Nucl. Med. 112 (1971) 682.

[74] FOLSE, R., BRAUNWALD, E., "Pulmonary vascular dilution curves recorded by external detection in the diagnosis of left to right shunts", Brit. Heart J. 24 (1962) 166.

[75] ROSENTHALL, L., "Nucleographic screening of patients for left-to-right cardiac shunts", Radiology 99 (1971) 601.

[76] ALAZRAKI, N. P., ASHBURN, W. L., HAGAN, A., FRIEDMAN, W. F., "Detection of left-to-right cardiac shunts with the scintillation camera pulmonary dilution curve", J. Nucl. Med. 13 (1972) 142.

[77] ADAM, W. E., SCHENCK, P., KAMPMANN, H., LORENZ, W. J., SCHNEIDER, W G., AMMANN, W., BILANIUK, L., "Investigation of cardiac dynamics using scintillation camera and computer", Medical Radioisotope Scintigraphy 2 (Proc. Symp. Salzburg, 1968) IAEA, Vienna (1969) 77.

[78] DEL GUERCIO, L. R. M., "Contrast dilution analysis", Trans. N. Y. Acad. Sci., Series II 33 (1971) 387.

[79] ISHII, Y., MacINTYRE, W. J., "Measurement of heart chamber volumes by analysis of dilution curves simultaneously recorded by scintillation camera", Circulation 44 (1971) 37.

[80] JONES, R. H., KLAPHAAK, B. A., SABISTON, D. C., JR., "Anatomic resolution in dynamic radionuclide studies by computer identification of radioactivity fluctuation with time", Proc. 2nd Symp. Sharing Computer Programs and Technology in Nuclear Medicine (Oak Ridge, Tennessee, 1972) USAEC Rep. CONF-720430 (1972) 151.

[81] FOLSE, R., BRAUNWALD, E., "Determination of fraction of left ventricular volume ejected per beat and of ventricular end-diastolic and residual volumes", Circulation 25 (1962) 674.

[82] BROOKS, R. C., VANDELINDE, V. D., HAMMERMEISTER, K. E., WARBASSE, J. R., "Digital filtering of left ventricular heart volume and calculation of aortic valve blood flow", Comput. Biomed. Res. 4 (1971) 340.

[83] ZARET, B. L., STRAUSS, H. W., HURLEY, P. J., NATARAJAN, T. K., PITT, B., "A noninvasive scintiphotographic method for detecting regional ventricular dysfunction in man", N. Engl. J. Med. 284 (1971) 1165.

[84] PARKER, J. A., SECKER-WALKER, R., HILL, R., SIEGEL, B. A., POTCHEN, E. J., "A new technique for the calculation of left ventricular ejection fraction", J. Nucl. Med. 13 (1972) 649.

[85] DODGE, H. T., SANDLER, H., BALLEW, D. W., LORD, J. D., JR., "The use of biplane angiocardiography for the measurement of left ventricular volume in man", Am. Heart J. 60 (1960) 762; DODGE, H. T., "Determination of left ventricular volume and mass", Radiologic Clinics of North America 9 (1971) 459.

[86] HUGENHOLTZ, P. G., WAGNER, H. R., SANDLER, H., "The in vivo determination of left ventricular volume", Circulation 37 (1968) 489.

[87] BECKENBACH, E. S., "The computerization of high speed cineangiocardiographic left ventricular volume determination", S. P. I. E. Seminar Proceedings 18 (1969) 173.

[88] KRISS, J. P., ENRIGHT, L. P., HAYDEN, W. G., WEXLER, L., SHUMWAY, N. E., "Radioisotopic angiocardiography: findings in congenital heart disease", J. Nucl. Med. 13 (1972) 31.

[89] WAGNER, H. N., JR., "Nuclear medicine in cardiovascular disease", Hospital Practice 7 (1972) 108.

[90] GOLDBERG, M. E., PONTO, R. A., LOKEN, M. K., "Radioisotope angiography" (in press, Radiology).

[91] PONTO, R. A., KUSH, G. S., LOKEN, M. K., "The use of a CDC-3300 computer for processing scintillation camera data in nuclear medicine", in Proceedings of Symposium on Sharing of Computer Programs and Technology in Nuclear Medicine, Oak Ridge, Tennessee (1971).

[92] SIGMAN, E. M., BENDER, M. A., BLAU, M., "Radiohippuran renography and radiohippuran renal autofluoroscopy", J. Urol. 92 (1964) 153.

[93] BRITTON, K. E., BROWN, N. J. G., "The renogram and its quantitation", Brit. J. Urol. Suppl. 41 (1969) 15.

[94] SHERWOOD, T., FREEMAN, T., JOEKES, A. M., "The clinical 'renogram' as a guide to renal function", Brit. J. Radiol. 37 (1964) 645.

[95] CONSTANTINIDES, C., KOSTAMIS, P., BINOPOULOS, D., DARSINOS, J., MALAMOS, B., "Radionuclide angiography for detection of relative differences in renal blood flow", in Dynamic Studies with Radioisotopes in Medicine (Proc. Symp. Rotterdam, 1970) IAEA, Vienna (1971) 321.

[96] LOKEN, M. K., LINNEMANN, R. E., KUSH, G. S., "Evaluation of renal function using a scintillation camera and computer", Radiology 93 (1969) 86.

[97] zum WINKEL, K., JOST, H., MOTZKUS, F., GOLDE, G., "Renal function studies with radioisotopes", in Dynamic Studies with Radioisotopes in Medicine (Proc. Symp. Rotterdam, 1970) IAEA, Vienna (1971) 229.

[98] KLOPPER, J. F., HAUSER, W., ATKINS, H. L., ECKELMAN, W. C., RICHARDS, P., "Evaluation of ^{99m}Tc-DTPA for the measurement of glomerular filtration rate", J. Nucl. Med. 13 (1972) 107.

[99] LADEFOGED, J., "Measurements of the renal blood flow in man with the ^{133}xenon wash-out technique", Scandinav. J. Clin. & Lab. Investigation 18 (1966) 299.

[100] DOLLERY, C. T., HUGH-JONES, P., MATTHEWS, C. M. E., "Use of radioactive xenon for studies of regional lung function: A comparison with oxygen", Brit. Med. J. 15 (1962) 1006.

[101] DE ROO, M. J. K., GORIS, M., VAN DER SCHUEREN, G., COSEMANS, J., BILLIET, L., GYSELEN, A., "Computerized dynamic scintigraphy of the lungs", Respiration 26 (1969) 408.

[102] BURDINE, J. A., ALAGARSAMY, V., RYDER, L. A., CARR, W. N., "Quantitative functional images of regional ventilation and perfusion", J. Nucl. Med. 13 (1972) 418.

[103] NEWHOUSE, M. T., WRIGHT, F. J., ENGHAM, G. K., "Use of scintillation camera and xenon-135 for study of topographic pulmonary function", Resp. Physiol. 4 (1968) 141.

[104] MacINTYRE, W. J., INKLEY, S. R., ROTH, E., DRESCHER, W. P., ISHII, Y., "Spatial recording of disappearance constants of ^{133}xenon washout from the lung", J. Lab. Clin. Med. 76 (1970) 701.

[105] MEDINA, J. R., LILLEHIE, J. P., LOKEN, M. K., EBERT, R. V., "Use of the scintillation Anger camera and xenon Xe^{133} in the study of chronic obstructive lung disease", J. A. M. A. 208 (1969) 985.

[106] HAYBITTLE, J. L., "The quantitative analysis of cerebral scintiscans", Phys. Med. Biol. 11 (1966) 474.

[107] AKERMAN, M., KOUTOULIDIS, C., "Cerebral angioscintigraphy using ^{99m}-technetium", Rev. Neurol. 122 (1970) 343.

[108] CRAWLEY, J. C. W., VEALL, N., "Gamma spectrum subtraction technique for measurement of activity in body organs and its use for cerebral blood flow studies", in Dynamic Studies with Radioisotopes in Medicine (Proc. Symp. Rotterdam, 1970) IAEA, Vienna (1971) 585.

[109] WALTZ, A. G., WANEK, A. R., ANDERSON, R. E., "Comparison of analytic methods for calculation of cerebral blood flow after intracarotid injection of ^{133}Xe", J. Nucl. Med. 13 (1972) 66.

[110] ASHKAR, F. S., SMITH, E. M., "The dynamic thyroid study", J. A. M. A. 217 (1971).

[111] RAMANTHAN, P., JOHNSON, D. E., CHOPRA, U., "Dynamic studies of thyroid function with the magna camera", J. Nucl. Med. 11 (1970) 640.

[112] WILLIAMS, E. D., GLASS, H. I., GOOLDEN, A. W. G., SATYAVANICH, S., "Comparison of two methods of measuring the thyroidal uptake of ^{99m}Tc", J. Nucl. Med. 13 (1972) 159.

[113] WAGNER, H. N., JR., NATARAJAN, T. K., "Computers in nuclear medicine", in Year Book of Nuclear Medicine (QUINN, J. L., III, Ed.) Year Book Medical Publishers, Chicago (1972) 5.

[114] DONATO, L., "Quantitative radiocardigraphy and myocardial blood flow measurements with radioisotopes", in Dynamic Studies with Radioisotopes in Medicine (Proc. Symp. Rotterdam, 1970) IAEA, Vienna (1971) 645.

[115] PARKEY, R. W., LEWIS, S. E., STOKELY, E. M., BONTE, F. J., "Compartmental analysis of the ^{133}Xe regional myocardial blood-flow curve", Radiology 104 (1972) 425.

[116] TAPLIN, G. V., "Dynamic Studies of liver function with radioisotopes", in Dynamic Studies with Radioisotopes in Medicine (Proc. Symp. Rotterdam, 1970) IAEA, Vienna (1971) 373.

[117] SABA, T. M., KAPLAN, E., GRAHAM, L., CORNELL, R. P., "Hepatic phagocytic, metabolic, and blood-flow evaluation by dynamic scintigraphy", J. Nucl. Med. 13 (1972) 300.

[118] ERICKSON, J. J., BRILL, A. B., "Physical considerations for dual radionuclide imaging techniques", in Quantitative Organ Visualization in Nuclear Medicine (KENNY, P. J., SMITH, E. M., Eds.) University of Miami Press, Coral Gables, Florida (1971) 777.

[119] SCHNECK, P., LANGE, D., SCHNABEL, K., AMMAN, W., SCHEER, K. E., "Qualitative and quantitative studies in simultaneous double-tracer investigations with a scintillation camera", J. Nucl. Med. 11 (1970) 642.

[120] BLANQUET, P., BECK, C., PIGNEUX, J., HECQUET, M. F., "Interet et limites de la scintigraphie pancreatique", pp. 707-719 in Medical Radioisotope Scintigraphy (Proc.Symp.Salzburg, 1968) IAEA, Vienna (1969).

[121] STAAB, E. V., BABB, O. A., KLATTE, E. C., BRILL, A. B., "Pancreatic radionuclide imaging using electronic subtraction technic", Radiology 99 (1971) 633-640.

[122] DESGREZ, A., RAZAFINDRAMAMBA, V., de SAINT-LAURENT, J., KELLERSHOHN, C., "Etude theorique et experimentale de la soustraction de deux images scintigraphiques: Application à la mise en evidence du pancréas", in Medical Radioisotope Scintigraphy 2 (Proc. Symp. Salzburg, 1968) IAEA, Vienna (1969) 677.

[123] BENDER, M., BLAU, M., BAKSHI, S., STEINBACK, J., "Value of radioisotope scanning for detection of pancreatic tumors", Cancer Bull. 22 (1970) 113.

[124] HATCHETTE, J. B., SHULER, S. E., MURISON, P. J., "Scintiphotos of the pancreas: analysis of 134 studies", J. Nucl. Med. 13 (1972) 51.

[125] HAMAMOTO, K., TORIZUKA, K., MUKAI, T., KOSAKA, T., SUZUKI, T., HONJYO, I., "Usefulness of computer scintigraphy for detecting liver tumor with ^{67}Ga-citrate and the scintillation camera", J. Nucl. Med. 13 (1972) 667.

[126] KAIHARA, S., NATARAJAN, T. K., WAGNER, H. N., JR., MAYNARD, C. D., "Construction of a functional image from regional rate constants", J. Nucl. Med. 10 (1969) 347.

[127] MacINTYRE, W. J., DRESCHER, W. P., INKLEY, S. R., "The future of functional scanning and its dependence on computer-assisted analysis", in Quantitative Organ Visualization in Nuclear Medicine (KENNY, P. J., SMITH, E. M., Eds.) University of Miami Press, Coral Gables, Florida (1971) 865.

[128] NATARAJAN, T. K., WAGNER, H. N., JR., "Functional imaging of regional ventilation and perfusion of the lungs", J. Nucl. Med. 13 (1972) 456.

[129] MacINTYRE, W. J., INKLEY, S. R., "Functional lung scanning with ^{133}xenon", J. Nucl. Med. 10 (1969) 355.

[130] KAKEHI, H., "Scan recording in color", Ch. 5 in Progress in Medical Radioisotope Scanning (KNISELEY, R. M., ANDREWS, G. A., HARRIS, C. C., Eds.) (Proc. Symp., Oak Ridge Institute of Nuclear Studies, 1962) Oak Ridge Institute of Nuclear Studies, Oak Ridge (1962).

[131] BEN-PORATH, M., CLAYTON, G. D., KAPLAN, E., Tape recording of dual-channel energy-modulated color scanning, J. Nucl. Med. 10 (1969) 155.

[132] LAUGHLIN, J. S., RITTER, F. W., DWYER, A. J., MAYER, K., GREENBERG, E. J, DIMICH, A. B, HASAN, S., ROTHSCHILD, E., MYERS, W. P. L., "Development and applications of quantitative and computer-analyzed counting and scanning", Cancer 25 (1970) 395.

[133] PLANIOL, TH., GARNIER, G., ITTI, R., BROCHIER, M., "La triscintigraphie cardiaque", Journal de Biologie et de Médicine Nucléaires 25 (1971) 3.

[134] ADAMS, R., JAFFE, H. L., "Recording scan data in photographic colour during live time", in Medical Radioisotope Scintigraphy 1 (Proc. Symp. Salzburg, 1968) IAEA, Vienna (1969) 331.

[135] ANGER, H. O., "Whole-body scanner Mark II", J. Nucl. Med. 7 (1966) 331.

[136] EVANS, R. C., "Radium poisoning II, The quantitative determination of the radium content and radium elimination rate in living persons", Am. J. Roentg. 37 (1937) 368.

[137] SORENSON, J. A., "Methods for quantitating radioactivity in vivo by external counting measurements", Ph. D. Thesis, University of Wisconsin (1971).

[138] GENNA, S., "Analytical methods in whole-body counting", in Clinical Uses of Whole-Body Counting (Proc. Panel, Vienna, 1965), IAEA, Vienna (1966) 37.

[139] OBERHAUSEN, E., ROMAHN, A., "Bestimmung der Nierenclearance durch externe Gamma-Strahlenmessung", p. 323 in Radiouklide in Kreislaufforschung und Kreislaufdiagnostik, 5. Jahrestagung der Ges. f. Nuklearmedizin, Vienna, 1967, Schattauer Verlag, Stuttgart (1968).

[140] TKOCZ, H-J, OBERHAUSEN, E., GLÖBEL, B., "Measurement of liver clearance rate with partially shielded whole body counter", p. 409 in Dynamic Studies with Radioisotopes in Medicine, IAEA, Vienna (1971), IAEA Rep. IAEA-SM-136/118.

TECHNICAL INFORMATION DIVISION
LAWRENCE BERKELEY LABORATORY
UNIVERSITY OF CALIFORNIA
BERKELEY, CALIFORNIA 94720